RÉPUBLIQUE ALGÉRIENNE DÉMOCRATIQUE ET POPULAIRE
MINISTÈRE DE L'ENSEIGNEMENT SUPÉRIEUR ET DE LA RECHERCHE SCIENTIFIQUE

ÉCOLE NATIONALE POLYTECHNIQUE

المدرسة الوطنية المتعددة التقنيات
Ecole Nationale Polytechnique

Département d'Électronique

End of Studies Project

Submitted for the fulfillment of State Engineer Degree in Electronics

---

Learning Based Artifact Removal for EEG and PPG signals

Contribution to artifact removal for EEG signals using Learning based methods

---

GUIR Abdelbaki

Under the supervision of

Prof. LALEG Taous-Meriem and **Prof. Latifa HAMAMI-MITICHE**

Presented and publicly defended on : Juin, 26^{th} 2024

Jury Members :

President :	Pr.BOUSBIA-SALAH Hicham	ENP, Algiers
Supervisor :	Pr.LALEG Taous Meriem	INRIA-Saclay, Paris
Co-Supervisor :	Pr.HAMAMI-MITICHE Latifa	ENP, Algiers
Examiner :	Dr.BOUADJENEK Nesrine	ENP, Algiers

ENP 2024

Électronique / ENP, 10 Rue des Frères OUDEK, El Harrach 16200 Alger Algérie.

RÉPUBLIQUE ALGÉRIENNE DÉMOCRATIQUE ET POPULAIRE
MINISTÈRE DE L'ENSEIGNEMENT SUPÉRIEUR ET DE LA RECHERCHE SCIENTIFIQUE

ÉCOLE NATIONALE POLYTECHNIQUE

المدرسة الوطنية المتعددة التقنيات
Ecole Nationale Polytechnique

Département d'Électronique

End of Studies Project

Submitted for the fulfillment of State Engineer Degree in Electronics

---

Learning Based Artifact Removal for EEG and PPG signals

Contribution to artifact removal for EEG signals using Learning based methods

---

GUIR Abdelbaki

Under the supervision of

Prof. LALEG Taous-Meriem and **Prof. Latifa HAMAMI-MITICHE**

Presented and publicly defended on : Juin, 26^{th} 2024

Jury Members :

President :	Pr.BOUSBIA-SALAH Hicham	ENP, Algiers
Supervisor :	Pr.LALEG Taous Meriem	INRIA-Saclay, Paris
Co-Supervisor :	Pr.HAMAMI-MITICHE Latifa	ENP, Algiers
Examiner :	Dr.BOUADJENEK Nesrine	ENP, Algiers

ENP 2024

Électronique / ENP, 10 Rue des Frères OUDEK, El Harrach 16200 Alger Algérie.

RÉPUBLIQUE ALGÉRIENNE DÉMOCRATIQUE ET POPULAIRE
MINISTÈRE DE L'ENSEIGNEMENT SUPÉRIEUR ET DE LA RECHERCHE SCIENTIFIQUE

ÉCOLE NATIONALE POLYTECHNIQUE

المدرسة الوطنية المتعددة التقنيات
Ecole Nationale Polytechnique

Département d'Électronique

Mémoire de Projet de Fin d'Études

Présenté en vue de l'obtention du diplôme d'Ingénieur d'État en Électronique

---

Élimination des Artéfacts Basée sur l'Apprentissage pour les Signaux EEG et PPG

Contribution à l'élimination des artéfacts pour les signaux EEG en utilisant des méthodes basées sur l'apprentissage

---

GUIR Abdelbaki

Sous la supervision de

Pr. LALEG Taous-Meriem et **Pr. Latifa HAMAMI-MITICHE**

Présenté et soutenu publiquement le : Juin, 26^{e} 2024

Membres du jury :

Président :	Pr. BOUSBIA-SALAH Hicham	ENP, Alger
Encadrante :	Pr. LALEG Taous Meriem	INRIA-Saclay, Paris
Co-Encadrante :	Pr. HAMAMI-MITICHE Latifa	ENP, Alger
Examinatrice :	Dr. BOUADJENEK Nesrine	ENP, Alger

ENP 2024

Électronique / ENP, 10 Rue des Frères OUDEK, El Harrach 16200 Alger Algérie.

الملخص

تستكشف هذه الدراسة استخدام أساليب التعلم العميق، خاصة الشبكات العصبية التلافيفية العميقة (Deep CNN) وشبكات التوليد التنافسية الدورية (Cycle GAN)، لتنقية الإشارات العصبية الفيزيولوجية مثل EEG و PPG من الشوائب غير المرغوب فيها. تتلوث إشارات EEG غالبا بالشوائب الكهربية العينية (EOG) والعضلية (EMG)، بينما تعاني إشارات PPG من تموجات الحركة وانجرافات الخط الأساسي. أظهرت نماذجنا تحسينا كبيرا في جودة الإشارة مقارنة بالتقنيات التقليدية، مما يسلط الضوء على إمكانية البنى العميقة للتعلم في تحسين معالجة الإشارات العصبية الفيزيولوجية وتطبيقات الطب الحيوي.

الكلمات المفتاحية:
مخطط كهربية الدماغ، تخطيط التحجم الضوئي، الشبكات العصبية التلافيفية، التعلم العميق، شبكات التوليد التنافسية الدورية، معالجة الصور، معالجة الإشارات.

Résumé

Cette étude explore l'utilisation de méthodes d'apprentissage profond, notamment les réseaux de neurones convolutifs profonds (Deep CNN) et les réseaux adversatifs génératifs cycliques (Cycle GAN), pour purifier les signaux neurophysiologiques EEG et PPG des artefacts indésirables. Les EEG sont souvent contaminés par des artefacts EOG et EMG, tandis que les PPG souffrent d'artefacts de mouvement et de dérives de la ligne de base. Nos modèles ont montré une amélioration significative de la qualité des signaux par rapport aux techniques traditionnelles, soulignant le potentiel des architectures d'apprentissage profond pour améliorer le traitement des signaux neurophysiologiques et les applications biomédicales.

Mots clés : électroencéphalogramme, photopléthysmographie, réseaux neuronaux convolutifs profonds, apprentissage profond, réseaux adverses génératifs cycliques, traitement d'images, traitement de signaux.

Abstract

This study explores the use of deep learning methods, particularly Deep Convolutional Neural Networks (Deep CNN) and Cycle Generative Adversarial Networks (Cycle GAN), to purify neurophysiological signals such as EEG and PPG from unwanted artifacts. EEG signals are often contaminated by EOG and EMG artifacts, while PPG signals suffer from motion artifacts and baseline drifts. Our models have shown a significant improvement in signal quality compared to traditional techniques, highlighting the potential of deep learning architectures to enhance the processing of neurophysiological signals and biomedical applications.

Keywords : electroencephalogram, photoplethysmogram, deep convolutional neural networks, deep learning, cycle generative adversarial networks, image processing, signal processing.

Acknowledgments

Before anything at all, I would love to express my sincere gratitude towards my project supervison Dr.Taous Meriem Laleg, Professor and permanent researcher with INRIA-Saclay, for her constant guidance and support, for her infinite kindness, gentleness and presence at all times, Her wealth of knowledge and infectious enthusiasm for engineering and mathematics consistently inspire admiration and motivation, The experience I acquired under your supervision in research is invaluable. I am incredibly fortunate to have had the privilege of learning under your guidance.

I would like to express once again my sincere gratitude towards my Co-supervisor Ms. Hamami-Mitiche Latifa, Professor with Ecole Nationale Polytechnique for her supervision, flexibility and constant love and support towards this projects. One of the wisest individuals i have ever met in my life. The amount of knowledge and kindess she shared me. All of that won't be forgettable.

I would like to thank the President of the jury Pr Bousbia-Salah Hichem, Professor with Ecole Nationale Polytechnique and the Examiner Bouadjenek Nesrine, Teacher-Researcher with Ecole Nationale Polytechnique for agreeing to be members of the reading committee and for their constructive analysis of the present work. A special thanks is dedicated to them for their time and teaching and support for the last three years.

Dedication

Everything i accomplished in this life, including this project. All is dedicated to my beloved Mom and Dad. Thank you for all the support.

I would like to express my gratitude to Ms.Sara Maria Nour Sadoun for her guide and support throughout this work, and for her kindess to me, to acquire the necessary skills to tackle this kind of projects. Thank you from the depth of ma heart˜

Special thanks to my dear friend Israel J Jesus Santos Filho, for his support during the toughest moments in this project, muito obrigado pelo apoio meu irmão.

Akram Farouk,you were always by ma side for every step i took. much love for you bud.

Finally, without forgetting the main support during the past 3 years my friends within the electronics engineering departement Abderehmane Foutia, Nadjib Rahal, Mehdi Chamess Eddine. Much love for your guys !

Table of contents

List of Figures

List of Tables

Acronyms list

- **CNN** : Convolutional Neural Network
- **DNN** : Deep Neural Network
- **AI** : Artificial Intelligence
- **GAN** : Generative Adversarial Network
- **PPG** : Photoplethysmograph
- **EEG** : Electroencephalograph
- **EMG** : Electromyogram
- **EOG** : Electrooculography
- **ECG** : Electrocardiogram
- **SNR** : Signal to Noise Ratio
- **ICA** : Independant Component Analysis
- **IVA** : Independant Vector Analysis
- **EEMD** : Ensemble Empirical Mode Decomposition
- **DWT** : Discrete Wavelet Transform
- **NIRS** : Functional near-infrared spectroscopy

General Introduction

In waves and pulses, life reveals its silent story, Through EEG's sparks and PPG's glowing glory. Electrodes whisper brainwaves' quiet might, While light and blood dance in PPG's soft light. A symphony of signals, a cadence of care, In biomedical fields, their truths lay bare. Unveiling secrets of the mind and heart, From neural paths to each beat's start. In the silent dialogue of pulse and brain, Life's hidden rhythms softly explain.

Electroencephalography (EEG) and Photoplethysmography (PPG) are pivotal non-invasive techniques in the biomedical field, used extensively for monitoring and diagnosing various physiological conditions. EEG captures the electrical activity of the brain through electrodes placed on the scalp, while PPG measures blood volume changes at the skin's surface using a light source and a photodetector. Despite their invaluable contributions to medical diagnostics and research, both EEG and PPG signals are susceptible to various artifacts that can significantly contaminate the recordings, complicating the analysis and interpretation of these signals.

Artifacts in EEG and PPG signals can originate from a variety of sources, including physiological activities (e.g., muscle movements, eye blinks, and heartbeats), environmental interferences (e.g., electromagnetic noise), and technical issues (e.g., electrode displacement). These artifacts can obscure the true physiological signals, leading to erroneous conclusions and misdiagnoses if not adequately addressed. For example, muscle artifacts in EEG can mimic or mask epileptic activity, while motion artifacts in PPG can distort heart rate and blood oxygen measurements.

Numerous studies have focused on the purification of EEG and PPG signals from these artifacts, employing various signal processing and machine learning techniques. Some notable works include the use of Independent Component Analysis (ICA) and Empirical Mode Decomposition (EMD) for EEG artifact removal, and adaptive filtering methods for PPG signal enhancement. However, recent advancements in deep learning have opened new avenues for more robust and accurate artifact removal.

This project aims to explore the use of Deep Convolutional Neural Networks (Deep CNN) and Cycle-Consistent Generative Adversarial Networks (CycleGAN) for the removal of artifacts from EEG and PPG signals. Our methodology leverages the powerful feature extraction capabilities of Deep CNNs and the strengths of CycleGAN to enhance the quality of these neurophysiological signals.

Main Contribution

This project makes several significant contributions to the field of biomedical signal processing, particularly in the removal of artifacts from EEG signals. The main added value of this research lies in the innovative use of Cycle-Consistent Generative Adversarial Networks (CycleGANs) to remove Electrooculogram (EOG) and Electromyogram (EMG) artifacts from EEG signals—a novel application that has not been explored before. The contribution relies on several key points :

- Transforming Artifact signals (EOG and EMG) to 2D representation.
- Preparing the proper CycleGAN dataset format.
- Evaluation for the performance.

- Discussion about future work.

Organization of the Dissertation

The structure of this project report is as follows :

- Chapter 1 : General Background on EEG and PPG Signals This chapter provides a comprehensive overview of EEG and PPG signals, detailing their physiological basis, common applications, and the types of artifacts that commonly affect these signals.

- Chapter 2 : State of the Art in Artifact Removal for Neurophysiological Signals This chapter reviews the current state of research in artifact removal, highlighting significant contributions and methodologies from recent literature. It includes a discussion of both traditional signal processing techniques and modern deep learning approaches.

- Chapter 3 : Our Methodology outlines the proposed methodology for artifact removal. It explains the design and implementation of Deep CNNs and CycleGAN for EEG, and CycleGAN for PPG. Detailed descriptions of the network architectures, training processes, and evaluation metrics are provided.

- Chapter 4 : This Chapter presents the experimental results obtained from applying the proposed methods to real-world EEG and PPG datasets. It includes quantitative and qualitative assessments of the artifact removal performance, comparisons with existing methods, and discussions on the implications of the findings.

By addressing the challenges posed by artifacts in EEG and PPG signals, this project aims to contribute to the enhancement of signal quality and reliability, thereby improving the accuracy of neurophysiological assessments and diagnoses.

Finally, we end this project with a general conclusion and future perspectives.

Chapitre 1

Artifacts in EEG and PPG signals

1.1 Introduction

Neurophysiological signals are critical in understanding and diagnosing various neurological and cardiovascular conditions. However, these signals are often contaminated by artifacts. This is particularly true for EEG and PPG, which have garnered significant interest from the research community due to the valuable information that can be extracted from them.

Both EEG and PPG signals are prone to artifacts that can arise from numerous sources, including muscle activity, eye movements, electrical interference, and poor sensor contact. These artifacts can lead to potential misinterpretations and incorrect diagnoses.

This section will delve into EEG and PPG signals, examine the specific challenges posed by various artifacts in their recordings, and discuss the techniques employed to minimize these artifacts and ensure reliable data acquisition.

1.2 Electroencephalography (EEG)

1.2.1 What is EEG ?

EEG is a technique used to monitor the electrical activity of the human brain over time. It plays a crucial role in studying brain functions and identifying neurological disorders. EEG recordings are invaluable for diagnosing conditions like epilepsy, brain tumors, head injuries, and dementia, as well as for managing behavioral issues such as autism and attention disorders. Hans Berger, a neuropsychiatrist from the University of Jena in Germany, introduced the first EEG recording machine in 1929, marking the beginning of neurophysiology as a distinct medical field.

In an EEG test, electrodes—small disks—are positioned at various points on the scalp using temporary adhesives. These electrodes are then linked in pairs to an amplifier and an EEG recording device, which translates the electrical signals into visible wavy lines.

Figure 1.1 showcases the placement of electrodes on the scalp for EEG signal recording, with the resulting signals displayed on a computer screen. These electrodes capture minute electrical charges generated by brain cell activity, which are then amplified and visualized on a graph.

There are two main types of EEGs, distinguished by where the signal is captured within the head :

- **Scalp EEG :** This involves placing small electrodes directly on the scalp, ensuring good me-

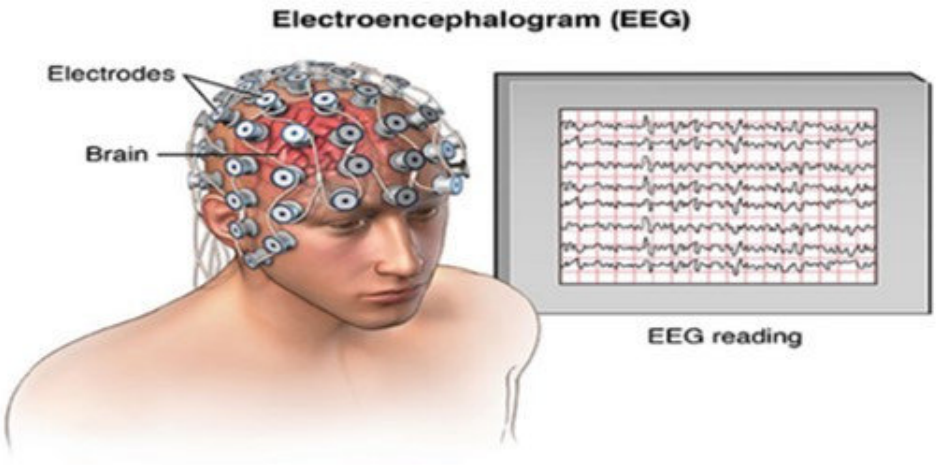

FIGURE 1.1 – An illustration of EEG recording, [3]

chanical and electrical contact.

- **Intracranial EEG :** In this method, special electrodes are surgically implanted into the brain.

The amplitude of an EEG signal typically falls within the range of 1 to 100 µV in a normal adult. However, when measured with subdural needle electrodes, it can be approximately 10 to 20 mV. Due to the nonuniform architecture of the brain and its functional organization, the EEG readings can vary depending on the specific location of the recording electrodes.

1.2.2 Electrodes placement

The positioning of electrodes is crucial because different lobes of the cerebral cortex are responsible for various types of activities. To address this, the international **10-20** electrode system is commonly used for localizing scalp electrodes.

In this system, the **10** and **20** denote the actual distances between adjacent electrodes, which are either 10% or 20% of the total front-back or right-left distance of the skull. The positions are determined by two key points :

- **nasion** : the midpoint between the forehead and the nose.
- **inon** : which is the bony prominence at the base skull on the midline at the back of the head.

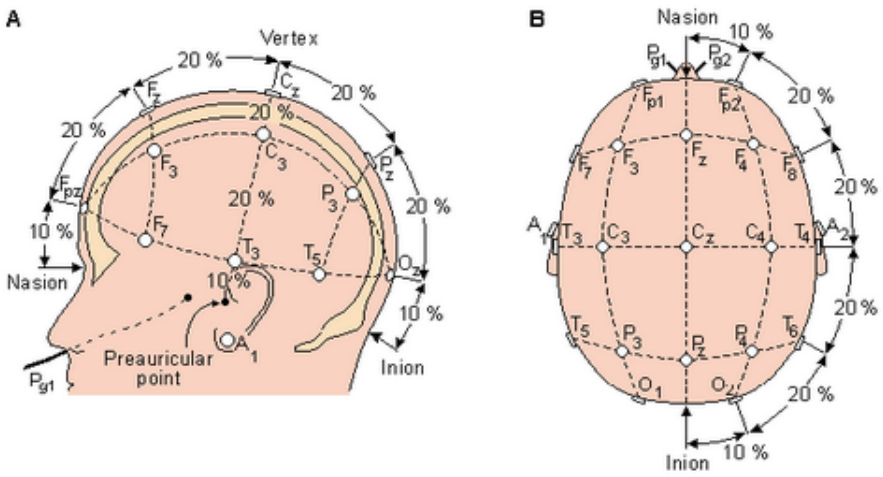

FIGURE 1.2 – An illustration of the international 10–20 electrode placement system. [44]

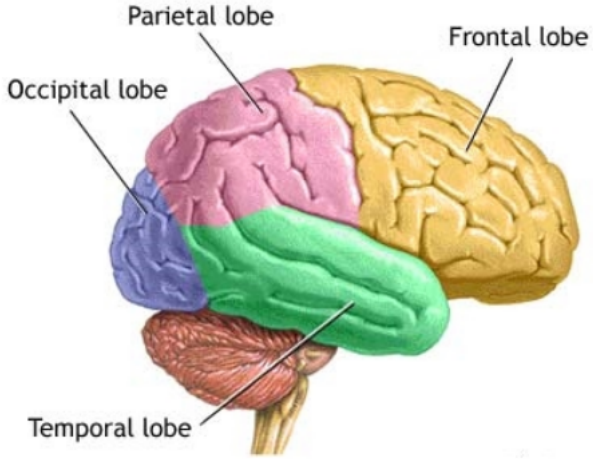

FIGURE 1.3 – Division of each lobe in the brain hemisphere [44]

Brain region/Cerebral lobe	Channel letter
Frontal	F
Parietal	P
Occipital	O
Temporal	T
Central	C
Front Polar	Fp
Auricular	A

Each location uses a letter to identify the brain lobes and regions as presented in Fig. 1.3 A number accompanies the letter in order to identify the hemisphere location. Odd numbers are used to refer to the electrodes positioned on the left hemisphere while the even numbers are for those on the right hemisphere. Instead of a number associated with the lobe letter, a “z” refers to an electrode placed on the midline.

Since an EEG signal measures the voltage difference between two electrodes, the EEG display on the reading machine can be configured in various arrangements. The arrangement of electrodes is called a montage.

1.2.3 Common EEG montages

Several EEG montages are available, each based on how the potential difference between two electrodes is calculated and displayed on the device. Among these montages, we include :

1.2.3.1 Referential montage

Every channel denotes the difference between a specific electrode and a chosen reference electrode. The reference electrode’s position isn’t standardized (in Fig.1.4, we use electrode A2 as the reference). Midline positions are commonly utilized as they don’t amplify the signal in one hemisphere versus the other.

Another common reference is "linked ears," which involves either a physical or mathematical averaging of electrodes attached to both earlobes and mastoids.

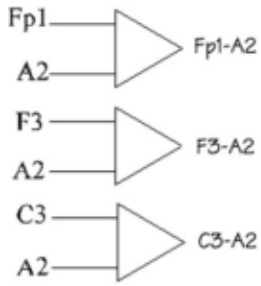

FIGURE 1.4 – An illustration for the referential montage [24]

1.2.3.2 Bipolar montage

A single channel is formed by a pair of electrodes, and each channel (or waveform) illustrates the voltage difference between two adjacent electrodes. The entire montage comprises a sequence of these channels. In Fig. 1.8, a diagram of a bipolar montage is depicted, where the channel **Fp1-F3** represents the voltage difference between the **Fp1** electrode and the F3 electrode. The subsequent channel in the montage, **F3-C3**, illustrates the voltage difference between **F3** and **C3**, and so forth, across all electrodes.

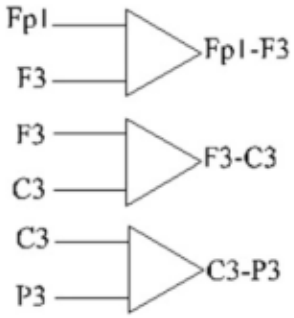

FIGURE 1.5 – An illustration for the bipolar montage [24]

1.2.3.3 Average reference montage

A different kind of montage which takes the signals from all the amplifiers and combines and amplifies them, resulting in a signal that serves as the common reference for each channel. see Fig.1.6

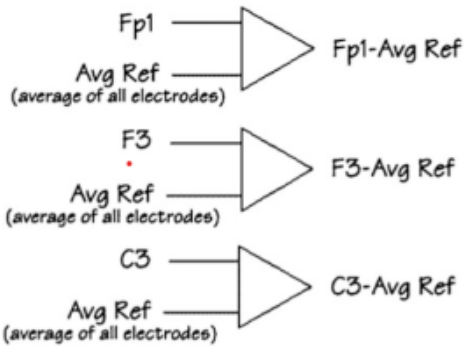

FIGURE 1.6 – An illustration for the average referential montage [24]

1.2.4 Brain Waves

Neural signals discharge rhythmically and spontaneously, highlighting their inherent spontaneity, which has opened up new avenues in EEG research. Among EEG features, the rhythmicity of spontaneous EEG is paramount, indicating its frequency diversity, alongside spatial characteristics. Currently, EEG can be categorized based on rhythm frequency into various types [10] :

1.2.4.1 Delta Waves

It includes both the **delta 1** rhythm **(1-2Hz)** and the **delta 2** rhythm **(2-4Hz)**, categorized as **non-major** rhythms primarily observed during deep sleep, anesthesia, or in the presence of organic brain lesions. The amplitude typically ranges from **20** to **200 µV**.

1.2.4.2 Theta Waves

The frequency within the range of **(4 -8 Hz)**, known as the **theta** rhythm, is observed bilaterally in the parietal and temporal lobes of younger individuals' brains. It manifests during states of drowsiness or when the central nervous system experiences inhibition.

1.2.4.3 Alpha Waves

The frequency range is between **(8 - 12 Hz)**. The alpha rhythm stands out as the most crucial aspect of the EEG signal, with its primary frequency typically around 10 Hz. It is prominently observed in the occipital region of the human brain (refer to Fig. 1.3). The amplitude of alpha waves typically falls between **20** and **100 µV**. The alpha rhythm predominantly reflects cognitive processing in the human body and is readily detectable, making it a focal point in EEG research.

1.2.4.4 Beta Waves

The frequency range falls between **(13 - 30 Hz)**, with an amplitude range of **5** to **20 µV**. This rhythm, often termed "fast" due to its higher frequency, is most prominent in the frontal and temporal lobes. It emerges in the brain during states of excitement.

1.2.4.5 Gamma Waves

Gamma waves are rapid oscillations exceeding **30 Hz**, typically observed during conscious perception. However, their small amplitude and susceptibility to contamination by **muscle artifacts** have led to them being underestimated and less widely studied compared to slower brain waves. High gamma activity in temporal regions is linked to memory processes, attention, working memory, and long-term cognitive functions. Moreover, it is implicated in psychiatric conditions like schizophrenia, Alzheimer's disease, and epilepsy.

Despite its significance, exploiting gamma frequency sub-bands using scalp EEG is challenging, and it is often excluded from EEG research unless invasive electrodes are utilized.

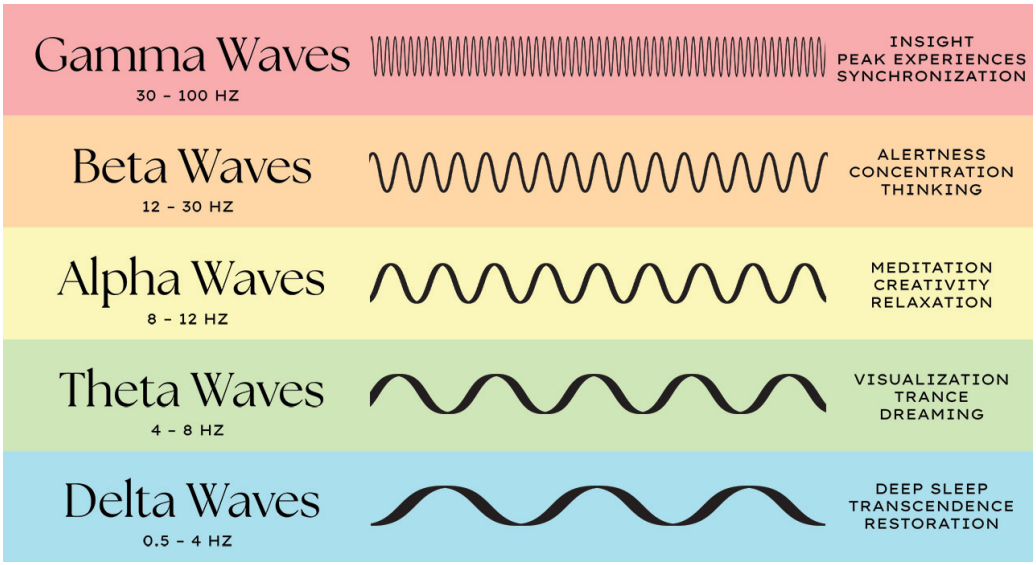

FIGURE 1.7 – Brain waves based on different frequency bands [38]

1.2.5 EEG artifacts

While the acquisition of EEG signals are often contaminated with several artifacts, which is going to make the interpretation and the analysis of the EEG signals to extract useful informations unfeasible. the following is a presentation for the different kinds of artifacts that occur while recording EEG signals.

1.2.5.1 Electromyogram (EMG)

Electromyogram (EMG) assesses the muscle's reaction or electrical activity when stimulated by a nerve. It is often used to diagnose neuromuscular disorders and to assess muscle function. Recording EEG is often obscured by EMG and complicate their analysis. [21]

1.2.5.2 Electrooculography (EOG)

Electrooculography (EOG) is a method used to measure the corneo-retinal standing potential present between the front and back of the human eye. The signal obtained from this measurement is referred to as the electrooculogram. EOG finds primary use in ophthalmological diagnosis and in tracking eye movements. thus EOG artifacts often appear as Eye mouvement artifacts in EEG signal, which corrupts it and makes it unreadable or almost impossible to analyze. [2]

1.2.5.3 Electrocardiogram (ECG)

Electrocardiography (ECG) is a graphical representation of the heart's electrical activity. This electrical activity is linked to changes in electrical potential of specialized cells responsible for contraction (myocytes) and cells specialized in generating and conducting impulses. It is collected by electrodes placed on the skin's surface. [45]

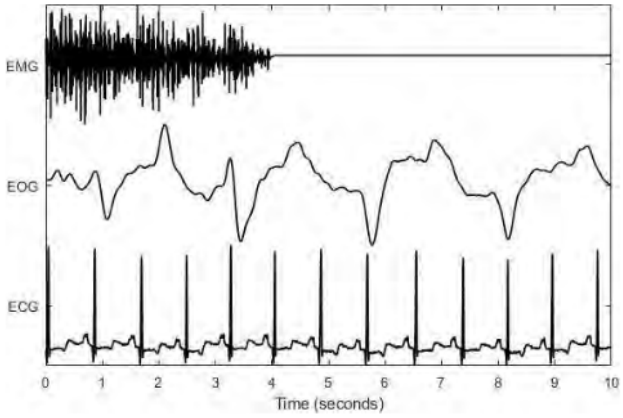

FIGURE 1.8 – Three kinds of artifacts EMG, EOG, and ECG [20]

1.2.6 Ensuring high EEG signal acquisition quality

In this subsection, we are going to present some of the techniques to ensure almost high quality EEG signals while recording.

1.2.6.1 Evaluation in time-domaine

We formulated two findings according to our anticipated signal quality in the time domain :

- *Finding 1 : The gel-based device exhibits a notably reduced prevalence of artifacts compared to the gel-free devices.*

Regarding the finding, the evalutation of the recorded EEG signals was conducted manually. Visual examination and subsequent removal of contaminated EEG segments by an expert is a widely practiced and widely accepted approach in both research and clinical environments. [42]

- *Finding 2 : The gel-based device demonstrates a notably superior signal-to-noise ratio **(SNR)** in comparison to the gel-free devices.*

Signal-to-noise ratio (SNR) serves as a standard technique for evaluating signal quality. SNR values were computed using the following formula 1 :

$$SNR = 10log_{10}(\frac{\sigma_x^2}{\sigma_s^2})[db] \tag{1}$$

Where, σ_x^2 is the variance of the signal and σ_s^2 is the variance of the noise.

1.2.6.2 Evaluation in frequency-domaine

To assess signal quality in the frequency domain. Our anticipation was that if a device exhibited good signal quality, we would observe significant disparities in the power values across different frequency bands during various tasks.

- *Finding 3 : In devices demonstrating high signal quality, we anticipate a notable Berger effect when comparing measurements taken with eyes open versus those taken with eyes closed.*[15]

This finding indicates that the power of the parietal alpha band is expected to decrease when the eyes are open compared to when they are closed. This phenomenon is commonly referred to as the **alpha block**.

- *Finding 4 : In devices exhibiting strong signal quality, we anticipate a noteworthy rise in frontal theta power when comparing less demanding cognitive tasks to more challenging ones.*

This hypothesis is based mainly on the dependency of the frontal theta band power on the experienced workload. Based on the results from numerous previous investigations.[41]

1.3 Photoplethysmogram (PPG)

1.3.1 What is PPG

Photoplethysmography (PPG) measures changes in the blood volume of a vascular tissue bed. Photoplethysmogram is a plethysmogram captured optically, useful for identifying fluctuations in blood volume within tissue microvessels.[11] [4]

FIGURE 1.9 – Pulse-oximeter device on a person index [5]

Typically, it's acquired using a pulse oximeter Fig.1.9, which emits light through the skin and gauges alterations in light absorption. This method allows for monitoring blood perfusion in the skin's dermis and subcutaneous tissue. see Fig.1.10

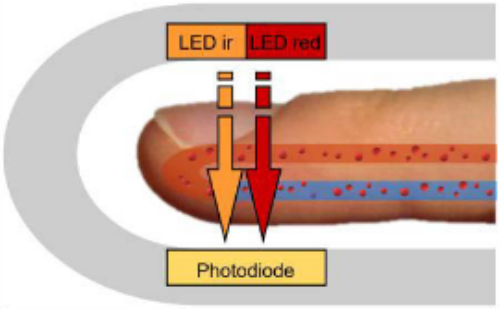

FIGURE 1.10 – Schematic of two LEDs transmitting light through a finger, which is then captured by the photodiode [27]

1.3.2 PPG signal acquisition

This subsection showcases the aspects of PPG sensor design required to ensure high-quality PPG signals.

Sensors types

Photoplethysmography is commonly conducted using **tissue-contact sensors** configured either in transmission (known as '**transillumination**') or reflection ('**adjacent**') mode Fig.1.11.[12]. A typical PPG sensor comprises a light emitter and a highly sensitive photodetector enclosed within a reusable spring-loaded clip. Light-emitting diodes (LEDs) are the preferred light sources in most cases . The photodetector commonly employed is a silicon photodiode, although other detectors like photocells and phototransistors are also utilized.[34]

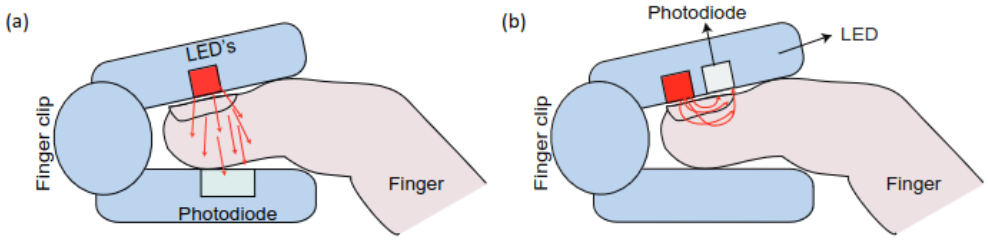

FIGURE 1.11 – (a) transmission mode, (b) reflectance mode.

The optoelectronics of the PPG sensor and its attachment mechanism to tissue serve as foundational elements in a PPG measurement system. Their design significantly affects signal quality, subsequent analysis of pulse waves, and the necessity for skilled noise reduction. Several other factors play a role in the design and selection of PPG sensors, such as determining whether reflection or transmission mode suits the intended application best, minimizing potential artifacts from ambient lighting including considerations for daylight filtering, positioning the digital interface relative to the sensor, ensuring safety, and considering aesthetics.

Maintaining adequate pressure at the probe-tissue interface is crucial. It should secure the PPG probe in place to minimize **movement artifacts** while avoiding excessive pressure that could distort the main features of the pulse wave.

1.3.3 PPG Pulse wave

Each PPG pulse wave comprises two discernible phases, as depicted in Fig 1.12 the anacrotic and catacrotic phases,[34] representing the rising and falling limbs, respectively.

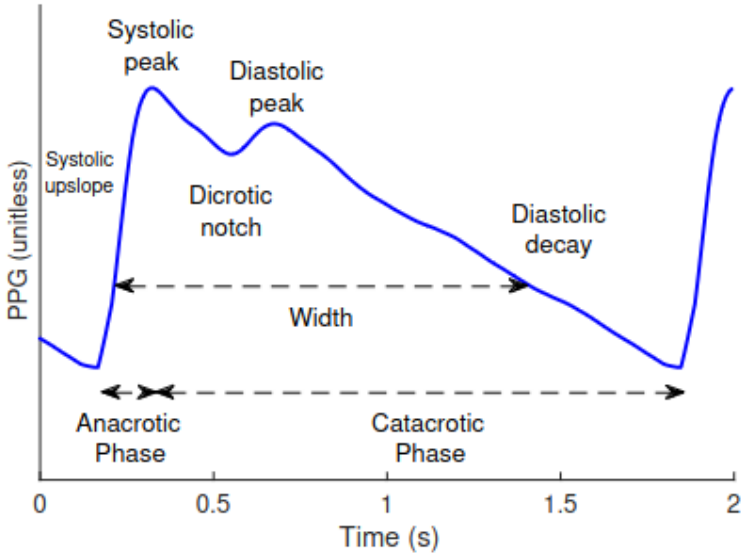

FIGURE 1.12 – he changes in PPG pulse wave shape which occur in healthy ageing. [34]

The morphology of the PPG pulse wave is shaped by various factors :

- **Heart Characteristics** : This includes parameters related to cardiac ejection, such as heart rate, heart rhythm, and stroke volume.
- **Circulatory System** : Properties of circulation, including arterial stiffness and blood pressure, influence the PPG waveform.
- **Additional Physiological Processes** : Factors like respiration and the autonomic nervous system, which can be affected by stress, also contribute to PPG waveform variations.
- **Disease** : Various diseases can impact the morphology of the PPG pulse wave, further adding complexity to its interpretation.

We should note that PPG pulse wave differs from person to person, age to age. Please see fig.1.13

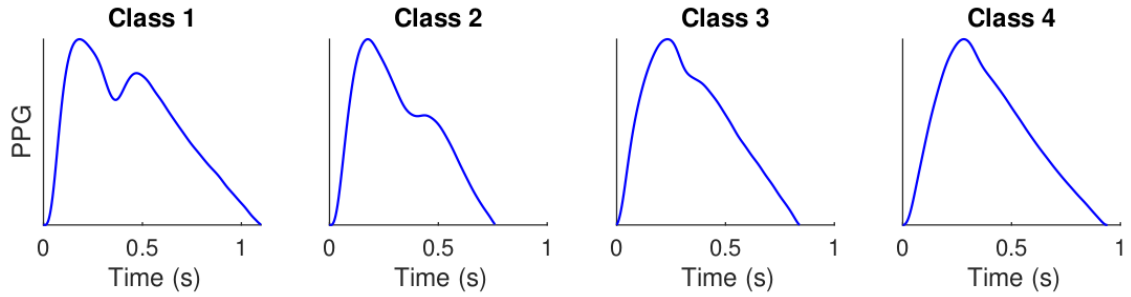

FIGURE 1.13 – In younger people (class 1), the pulse wave in PPG usually shows a peak during the relaxing phase of the heart (diastolic peak). However, as people get older (higher classes), this peak tends to become less prominent.[34]

1.3.4 PPG Artifacts

Artifacts in photoplethysmography (PPG) signals are unwanted disturbances or anomalies that can arise during signal acquisition and processing, potentially compromising the accuracy and reliability of physiological measurements. Here are some common types of artifacts in PPG signals :

1.3.4.1 Baseline Drift

Baseline drift refers to gradual changes in the baseline level of the PPG signal over time, unrelated to physiological variations. It can result from factors such as sensor displacement, changes in ambient light, or variations in skin perfusion. Baseline drift can obscure the underlying PPG waveform and affect the accuracy of measurements, requiring correction methods to restore signal integrity.

1.3.4.2 Motion artifacts

Motion artifacts occur due to movement or motion of the body, such as muscle contractions or limb motion. This kind of artifacts manifests as irregular fluctuations or distortions in the PPG waveform, making it challenging to extract accurate physiological information. However these artifacts are often mitigated using signal processing techniques or by ensuring sensor stability and proper positioning.

In our case of study we propose to investigate removing these artifacts using deep neural networks.

1.3.4.3 Hypoperfusion artifacts

Hypoperfusion, or reduced blood flow to tissues, affects photoplethysmography (PPG) signals by causing several distinct changes. In PPG waveforms, hypoperfusion is often marked by decreased signal amplitude, resulting in weaker and less pronounced pulsatile signals. Additionally, systolic peaks may be attenuated, and the onset of the pulsatile component may be delayed due to reduced blood flow dynamics. Hypoperfusion can also distort the shape and morphology of the waveform, leading to flattened or irregular patterns. Finally, increased baseline drift and noise may accompany hypoperfusion, complicating signal interpretation. Recognizing these changes in PPG signals is vital for accurately assessing tissue perfusion status in clinical and monitoring contexts.

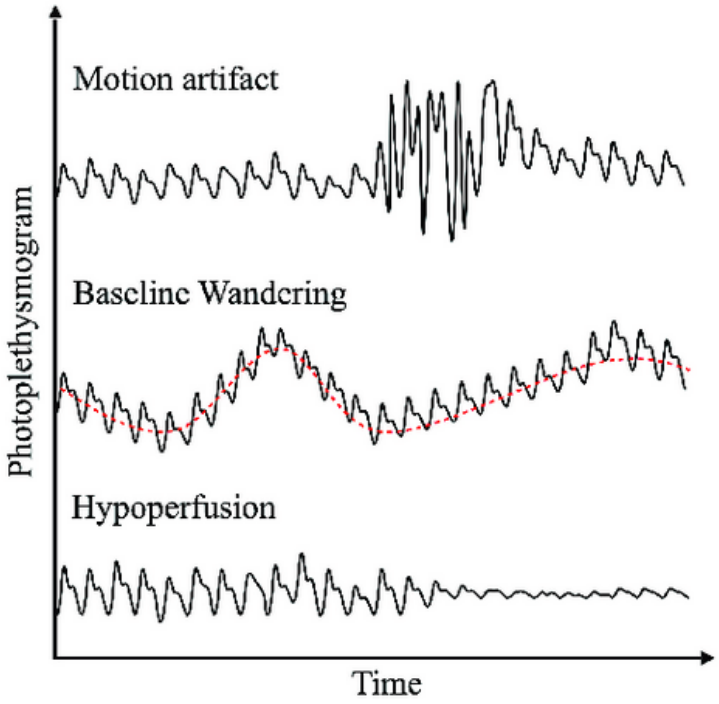

FIGURE 1.14 – Examples of representative PPG distortion due to motion artifact, baseline wandering, and hypoperfusion (from top to bottom).[37]

1.3.5 Ensuring high PPG signal acquisition quality

In this subsection, we present some of the techniques which ensure high quality PPG signals while recording.

- **Proper Sensor Placement :** Ensure that the PPG sensor is correctly positioned on the measurement site, typically a fingertip, earlobe, or other suitable peripheral area. Secure the sensor snugly but comfortably to minimize motion artifacts and ensure good skin contact for optimal light transmission.
- **Stable Environment :** Control environmental factors such as ambient light, temperature, and humidity to minimize their impact on the PPG signal. Shield the sensor from direct sunlight and sources of electrical interference to prevent signal distortion.
- **Motion Artifact Mitigation :** Minimize movement and muscle contractions during signal acquisition to reduce motion artifacts. Instruct the subject to remain still and relaxed during data collection, and use motion-resistant sensor designs or signal processing techniques to mitigate artifact effects.
- **Optimal Sensor Configuration :** Choose PPG sensor configurations and wavelengths that are suitable for the intended application and measurement site. Consider factors such as sensor

type (reflectance or transmittance), light source intensity, and wavelength selection to optimize signal quality and depth of tissue penetration.

- **Signal Processing Techniques :** Employ signal processing algorithms and techniques to enhance signal quality and remove noise and artifacts. This may include filtering methods, baseline drift correction, artifact detection, and motion artifact removal algorithms tailored to the specific characteristics of PPG signals.
- **Calibration and Validation :** Calibrate PPG devices regularly to ensure accurate and consistent measurements. Validate signal quality and device performance using reference standards or physiological validation methods to confirm the reliability of acquired data.
- **Subject Preparation :** Prepare subjects adequately before signal acquisition by ensuring proper hydration, minimizing caffeine and nicotine intake, and avoiding factors known to affect peripheral circulation. These measures can help optimize vascular tone and blood flow for improved signal quality.
- **Continuous Monitoring :** Continuously monitor signal quality during data acquisition to identify and address any issues in real-time. Visual inspection of signal waveforms, feedback from the subject, and automated quality control checks can help ensure the integrity of acquired PPG data.

1.4 Conclusion

Accurate interpretation of EEG and PPG signals hinges on effectively managing artifacts. By understanding the different types of artifacts that can contaminate these recordings, researchers can develop and implement appropriate mitigation strategies.

Fortunately, a vast array of techniques exist already to address these challenges. The next section delves into the existing literature, exploring the various methods and approaches employed to remove artifacts from EEG and PPG signals. We also present their advantages and limitations in different scenarios.

Chapitre 2

State of the art on artifact removal for EEG and PPG signals

2.1 Introduction

The quest for accurate and reliable information from Electroencephalogram (EEG) and Photoplethysmography (PPG) signals is hampered by artifacts – unwanted distortions that mask the underlying physiological data. This chapter tackles this challenge head-on by delving into the state-of-the-art in artifact removal techniques for both EEG and PPG signals.

Our exploration will navigate the existing literature, uncovering the ingenious algorithms that researchers have developed to combat these challenges. This review will equip you with a thorough understanding of the current landscape in EEG and PPG artifact removal.

2.2 EEG artifact removal

2.2.1 ICA based artifact detection

Independent Component Analysis (ICA) is a computational technique designed to decompose a multivariate signal into distinct additive subcomponents. Developed by Jeanny Hérault and Christian Jutten in 1985, ICA operates under the assumption that, at most, one subcomponent exhibits a Gaussian distribution, and all subcomponents are statistically independent of one another. ICA is a specific instance of blind source separation, with a classic application being the resolution of the "cocktail party problem," where it is used to isolate one person's speech amidst background noise in a crowded room.[22]

Central limit theory

The central limit theorem (CLT) states that, given suitable circumstances, when the sample mean is standardized, its distribution tends towards a standard normal distribution. This principle remains valid regardless of whether the initial variables follow a normal distribution or not. Various versions of the CLT exist, each pertinent to distinct conditions.

EEG components are known to be unique from each other, which means that artifacts have unique topographies and shapes [23], thus the detection would be the comparison between the components and the ground truth of the artifical artifacts, please see figure 2.5.

How ICA works : Let's imagine a mixture of two signals A, B 'we can generate these two signals with a simple python code (see figure 2.1)

```
import numpy as np
import matplotlib.pyplot as plt


A = np.sin(np.linspace(0, 50, 1000))
B = np.sin(np.linspace(0, 37, 1000) + 5)

# Plot A
plt.figure()
plt.plot(x_values_A, A, label='A')
plt.xlabel('X values')
plt.ylabel('sin(x)')
plt.legend()
plt.title('Sine function A')

# Plot B
plt.figure()
plt.plot(x_values_B - 5, B, label='B', color='red')
plt.xlabel('X values')
plt.ylabel('sin(x)')
plt.legend()
plt.title('Sine function B')

plt.show()

A = np.sin(x_values_A)
B = np.sin(x_values_B)

# Plot A and B
plt.plot(x_values_A, A, label='A')
plt.plot(x_values_B - 5, B, label='B')
plt.xlabel('X values')
plt.ylabel('sin(x)')
plt.legend()
plt.title('Sine functions A and B')
plt.show()
```

FIGURE 2.1 – Python code to generate the two signals

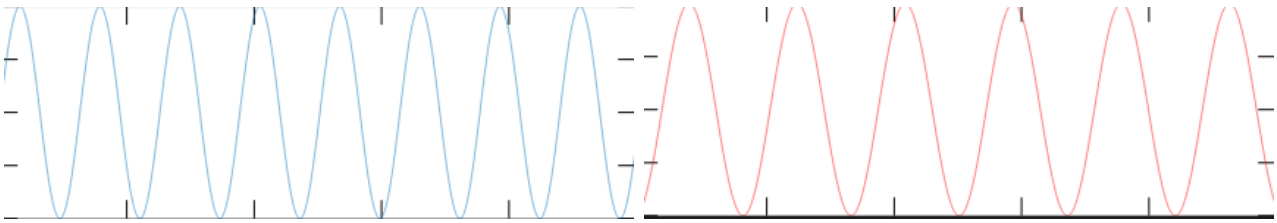

FIGURE 2.2 – (A), (B) : Blue, Red signals respectively, generated using the python code 2.1,

Now, we mix the signals linearly, first combination is $A - B$, second one is $1.73 * A + 3.41 * B$, (see figure 2.3)

Now lets apply fastICA to separate the mixtures. and get the following result 2.4

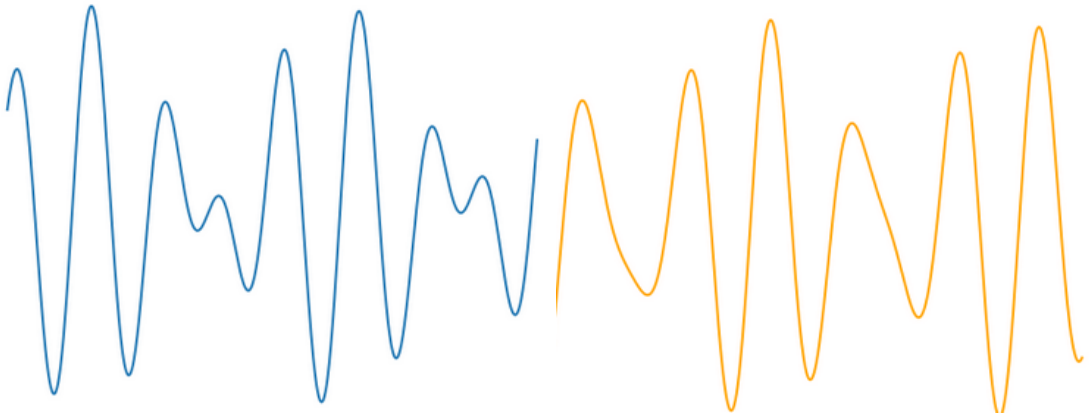

FIGURE 2.3 – $A - B$: blue and linear combination : orange.

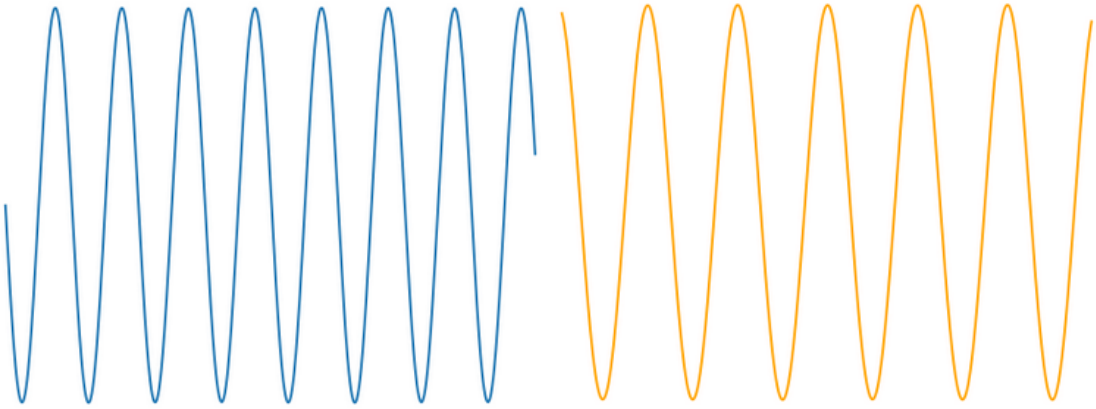

FIGURE 2.4 – independant components 'separated mixtures'.

To put ICA in the context of separating biomedical signals, we imagine n-electrodes recording array as n-dimensional space. CLT states that the linear mixture of these n-electrodes recordings arrays converge to a gaussian distribution. We project these signals on each basis axes, ICA rotates these axes in a way the probability density function is non-gaussian as possible. Thus the independance of each axis and the minimization of the mutual information. [17]

The separated components of the EEG signal may by generated inside or outside the brain, for instance eye blinks and muscular activities give unique independant component, with specific activities, Thus ICA performs the best in separating the sources. [31]

The paper [23] tested other methods such as Second order Blind identification that was developped by Prof. Adel Belouchrani et al. [14], which exploits the temporal correlations in the sources.They introduced several artificial artifacts such as Linear trends, high frequency events modelling temporal muscle artifacts (Figure 2.5) However the results of the paper utilized only Fast-ICA because it performed the best. (Figure 2.6).

2.2.2 Canonical Correlation Analysis (CCA)

In some studies, a Canonical Correlation Analysis was introduced as a multivariate generalization of the ordinary Pearson correlation [28]. EEG recordings are often contaminated by muscular artifacts that could make EEG interpretation unfeasible, or almost impossible [18]. The same study in the issue of cancelling muscular artifacts for single-channel EEG shown that mobility artifacts tend to have a low auto-correlation in contrast to clean EEG signals. thus CCA exploits this, and outperforms ICA in EMG noise cancellation.

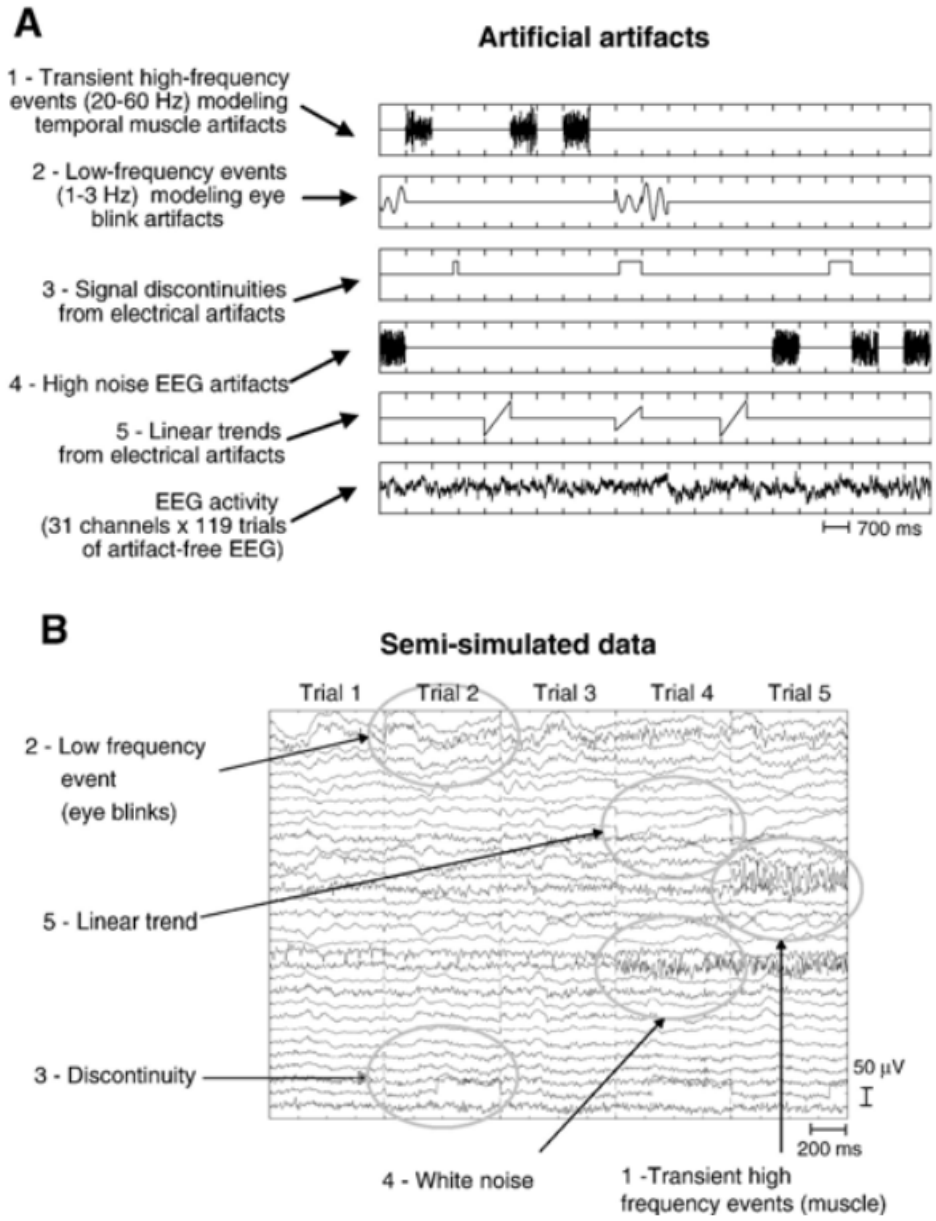

FIGURE 2.5 – (A) Types of artifcial artifacts introducted into actual EEG data (B) [23]

How CCA works : Let's Consider two zero mean random vectors $X = [x_1, x_2, ..., x_p]^T$ and $Y = [y_1, y_2, ..., y_q]^T$ of dimensions p and q where these two tells the number of channels used. CCA here aims to find linear combinations of both **X** and **Y** channels that have the maximum correlation coefficient with each other [28]. This leads to the following objective function with constraints :

$$\max_{v_1, v_2} \quad (v_1^T X_1 X_2^T v_2)^2$$
$$s.t. \quad v_1^T X_1 X_1^T v_1 = 1, \quad v_2^T X_2 X_2^T v_2 = 1$$

where $v_i's \quad (i = 1, 2)$ are the weight vectors.

Straightforwardly, the solution for this problem is to determine the eigenvectors of the matrices $\boldsymbol{(X_1 X_1^T)^{-1} X_1 X_2^T (X_2 X_2^T)^{-1} X_2 X_1^T}$ and $\boldsymbol{(X_2 X_2^T)^{-1} X_2 X_1^T (X_1 X_1^T)^{-1} X_1 X_2^T}$, respectively. the canonical variates **CV** $U_i's \quad (i = 1, 2)$ can be calculated directly from the original matrices $X_i's$ as $U_i = V_i^T X_i$. The corresponding rows of U_1 and U_2 are highly correlated, while the rows within each individual U_i are uncorrelated with each other. [18].

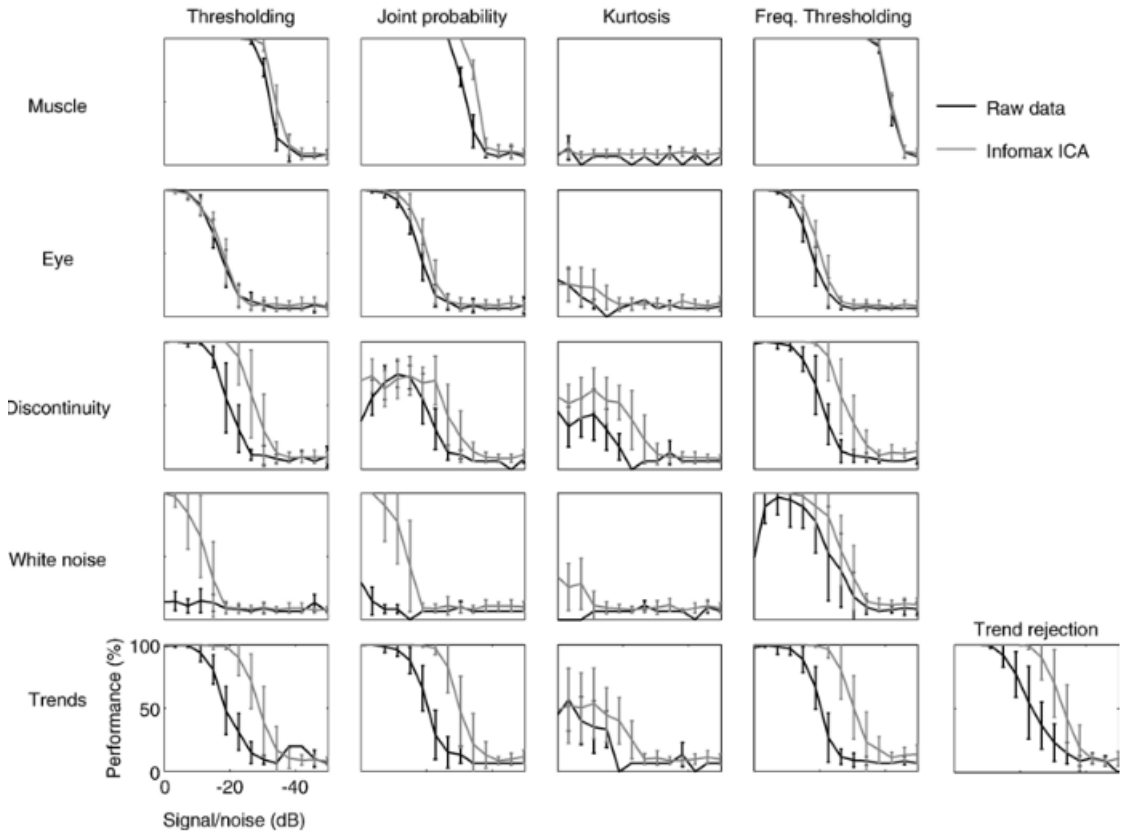

FIGURE 2.6 – Artifact detection performance with 5 different methods [Thresholding, Joint Probability, Kurtosis, Freq. Thresholding and Trend rejection].

Black traces : For each form of artifact, the five approaches were first optimally applied to the best single-channel data.
Grey traces : Infomax ICA computed the best single independent components from the data using the same procedures.
The vertical error bars display the performance variance over 20 replications, expressed as ± 1. Overall, spectral thresholding methods (right) performed best for artifacts less than 40 dB below the EEG in power, and all detection methods performed better when applied to the independent component data. [23]

CCA is further extended to separate artifacts from desired signals in a functional magnetic resonance imaging **(fMRI)** study under the assumption of that the source components are maximally auto-correlated and mutually uncorrelated [25], with that been said let X_1 be the observed data matrix X with P mixtures and T samples, and let X_2 be a temporally delayed version of the original data matrix $X_2(t) = X(t-1)$. Thus, CCA can separate the recorded data into the self-correlated and mutually uncorrelated sources. As a potential alternative for the most widely used ICA method, CCA has been previously tested with a number of ICA algorithms. The CCA-based methods were shown to outperform the ICA-based techniques for **EEG/fNIRS** artifact removal [43] [36]. To investigate the performance of this method (CCA) and perform a possible comparison against (ICA). Authors in [36] have recorded EEG signals for 15 subjects, each subject was asked again to record signals while doing several activities including chewing, frowning, eye mouvements, and blinking. resulting synthesised signals are made by mixing EEG signals and those when doing activities (EOG) and (EMG), for this ICA and CCA were applied to asses the performance between the two algorithms. Results are illustrated in Fig.2.7

Mathematically speaking, we can describe the synthesized signal using the following equation :

$$B_{syn} = B_{eeg} + \epsilon B_{emg}$$

where B_{eeg} ,B_{emg} are the clean EEG signals and muscle artifacts signals respectivley. and ϵ is the contribution of muscle artifacts to EEG signal.

To assess the performance Relative Root Mean Squared Error **(RRMSE)** was used as evaluation metric between **ICA** and **CCA** :

$$RRMSE = \frac{RMS(B_{eeg} - \hat{B})}{RMS(B_{eeg})},$$

where $RMS(x) = \sqrt{\frac{1}{T}xx^T}$, and $\hat{B}$ is the estimated EEG signal after muscular artifact cancellation. [19]

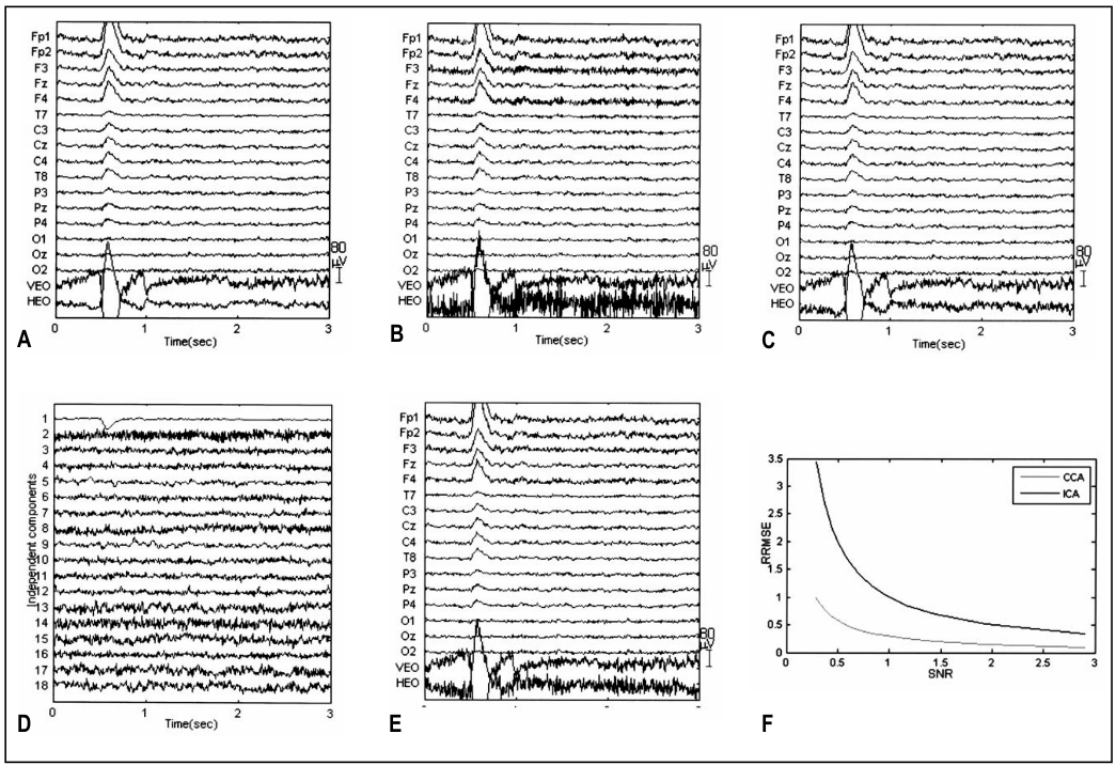

FIGURE 2.7 – Comparing the outcomes of EMG artifact removal using both CCA and ICA methods involved several steps : (A) $B_{\mathbf{eye}}$. (B) Generating Synthesized signal $B_{\mathbf{syn}}$ (η) where η=1. (C) Obtaining the reconstructed signal $B_{\mathbf{eye}}$ through CCA application. (D) Decomposing Signal $B_{\mathbf{syn}}$ (η) into 18 components via ICA. (E) Reconstructing Signal $B_{\mathbf{eye}}$ by eliminating IC2. (F) Evaluating the Relative Root Mean Square Error (RRMSE) of various algorithms at varying Signal-to-Noise Ratios (SNR). [36]

2.2.3 Independant Vector Analysis

Independant Vector Analysis (IVA) is an extension of (ICA) from one to several Datasets, In [13] IVA was formulated as general Joint Blind Source Separation (JBSS) framework to ensure that the extracted sources from each dataset are independant and perfectly correlated across different datasets.[19]

How IVA works : Let's denote $\boldsymbol{M}$ the number of datasets, each containing $\boldsymbol{P}$ samples. In IVA there is a concept to be defined which is the concept of Source Component Vector (SCV) across multiple datasets. therefore the p^{th} SCV, $s_p = [s_p^{[1]}, s_p^{[2]}, s_p^{[3]}, ..., s_p^{[M]}]$, the symbol $s_p^{[M]}$ $(m = 1, 2, ..., M)$ represents the p^{th} underlying source component in the m^{th} dataset. The goal of IVA is to identify the independent SCVs from multiple multidimensional datasets. This can be achieved by minimizing the

mutual information among the estimated SCVs $\hat{s_p}$'s :

$$I_{IVA} \triangleq I[\hat{s_1}; \hat{s_2}; \hat{s_3}; ....; \hat{s_P}] = H[\hat{s_P}] - H[\hat{s_1}; \hat{s_2}; \hat{s_3}; ....; \hat{s_P}],$$

where H denotes the entropy. By solving the above optimization problem, each estimated SCV $\hat{s_p}$ is independent of all other estimated SCVs, and meanwhile, the components within each SCV are dependent, e.g., $s_p^{[1]}$, and $s_p^{[2]}$ are highly correlated.

The implementation algorithms involve the selection of specific probability distributions for the SCVs. The most popular methods include IVA-L [30] and IVA-G [13].

IVA-L assumes that each Source Component Vector (SCV) conforms to a multivariate Laplace distribution, with isotropic properties and no second-order correlation. On the other hand, IVA-G leverages second-order statistical cues across datasets, assuming a multivariate Gaussian distribution for each SCV. While certain applications, like frequency domain Blind Source Separation (BSS) for speech recognition, may involve minimal second-order information across datasets, others, such as group fMRI studies, are anticipated to exhibit substantial correlation. This study employs IVA-G to capitalize on the significance of second-order information, particularly in capturing the temporal structure of muscular artifacts. Analogous to Canonical Correlation Analysis (CCA), IVA can segregate recorded data into self-correlated and mutually independent sources. One potential advantage of IVA over CCA lies in its ability to extract independent sources rather than merely uncorrelated ones through the utilization of Higher Order Statistics (HOS). However, this comes at the cost of increased computational complexity. Additionally, IVA assumes specific distributions for the underlying sources, which might not always hold true in practical scenarios.[19]

2.2.4 Ensemble Empirical Mode Decomposition

Ensemble Empirical Mode Decomposition (EMD) is a technique for analyzing signals with time-varying characteristics and complex interactions, using only one channel of data.[29]

How EMD works : EMD breaks down a signal into a set of basic building blocks called Intrinsic Mode Functions (IMFs). These IMFs capture the various oscillatory components within the signal, ranging from rapid fluctuations to slower trends. Each IMF follows two key principles [29] :

- The number of peaks and dips (extrema) is either very close to, or exactly matches, the number of times the signal crosses zero.[19]
- the mean value of the envelope defined by the local maxima and the envelope defined by the local minima is zero.[19]

EMD uses a special process called sifting to extract individual IMFs from the original signal (denoted by x). This process starts by finding all the peaks and valleys, technically known as extrema, within the signal.[29]

All local maximum points are connected by a cubic spline line to form the upper envelope e_u, Additionally, all local minimum points are connected similarly to form the lower envelope e_l the mean of e_u and e_l, a_1 is calculated as :

$$a_1 = \frac{e_u + e_l}{2}.$$

The difference between the signal and the mean is defined as the first component h_1 as :

$$h_1 = x - a_1.$$

In the second sifting process, h_1 is treated as the signal, and the mean a_{11} of its local maxima and local minima is found. We then have[19] :

$$h_{11} = h_1 - a_{11}.$$

Subsequently, we can repeat this sifting procedure $\boldsymbol{k}$ times until h_{1k} is an **IMF**, with :

$$h_{1k} = h_{1k\text{-}1} - a_{1k}.$$

Therefore, the first **IMF** component derived from the original signal is designated as :

$$c_1 = h_{1k}.$$

EMD relies on a specific rule to determine when the sifting process for an IMF is complete. This rule involves calculating the standard deviation (SD) of the difference between two successive sifting steps. The sifting process stops when this standard deviation falls below a certain threshold.

$$SD = \sum_{t=1}^{T} \left\{ \frac{[h_{1k\text{-}1}(t) - h_{1k}(t)]^2}{h_{1k\text{-}1}^2(t)} \right\}.$$

A typical value for SD can be set between 0.2 and 0.3 [29].

To extract the 2nd **IMF** component, we remove c_1 from the original signal x :

$$r_1 = x - c_1. \qquad (\star)$$

The residual r_1 is treated as a new signal, and the same sifting process is applied to obtain the 2nd **IMF** component c_2 and the residual :

$$r_2 = r_1 - c_2,$$

his procedure is repeated on the subsequent residuals r_j's, until the final residual r_J no longer contains any oscillation information,[19]

$$r_j = r_{j-1} - c_j. \qquad (\star\star)$$

By summing up Equations $\star$, $\star\star$, we obtain :

$$x = \sum_{j=1}^{J} c_j + r_J.$$

Thus, we decompose the original signal x into J empirical modes c_j 's and a residue r_J.

While the standard EMD algorithm struggles with noise, a recent improvement called EEMD offers a solution. Developed by Huang et al. [50], EEMD tackles noise by averaging the results from multiple analyses (ensemble). In each analysis, a copy of the original signal is combined with a random white noise signal of a specific strength. Even though individual analyses might be affected by noise, when the results are averaged across a sufficient number of trials (typically 10 or more), the random noise cancels out because it's assumed to be independent in each analysis. This approach keeps the computational cost reasonable. The recommended strength for the added noise is empirically set to 20% of the original signal's standard deviation.

2.2.5 EEMD-ICA

The idea of using EEMD with ICA to separate sources from single-channel recordings was introduced in [35]. This method aimed to remove unwanted signals like muscle activity (EMG) from brain activity (EEG) recordings. While this approach achieved limited success, it remains the only documented work on single-channel artifact removal in EEG data that we found.

Here's how the method works : EEMD is first used to decompose the single-channel recording (x) into multiple Intrinsic Mode Functions (**IMFs**), essentially creating a multi-channel signal (matrix X). This matrix is then fed into an algorithm called ***FastICA*** to extract the underlying source signals (estimated sources denoted by $\hat{S}$). Since some sources might represent artifacts, the corresponding rows in the $\hat{S}$ matrix can be removed. The remaining source matrix is then transformed back using the original mixing conditions (represented by matrix A) to obtain cleaned multi-channel signals (denoted by $\hat{X}$). Finally, by summing the recovered **IMFs** in $\hat{X}$ a single-channel recording $\hat{X}$ free from artifacts is ideally obtained.

2.2.6 Deep Learning approaches

Various deep learning techniques exists to to remove different kinds of artifacts from EEG signals, for instance,[32] used the ***U-Net*** architecture.Fig 2.8, where their EEG data was contaminated with **EOG** artifacts.

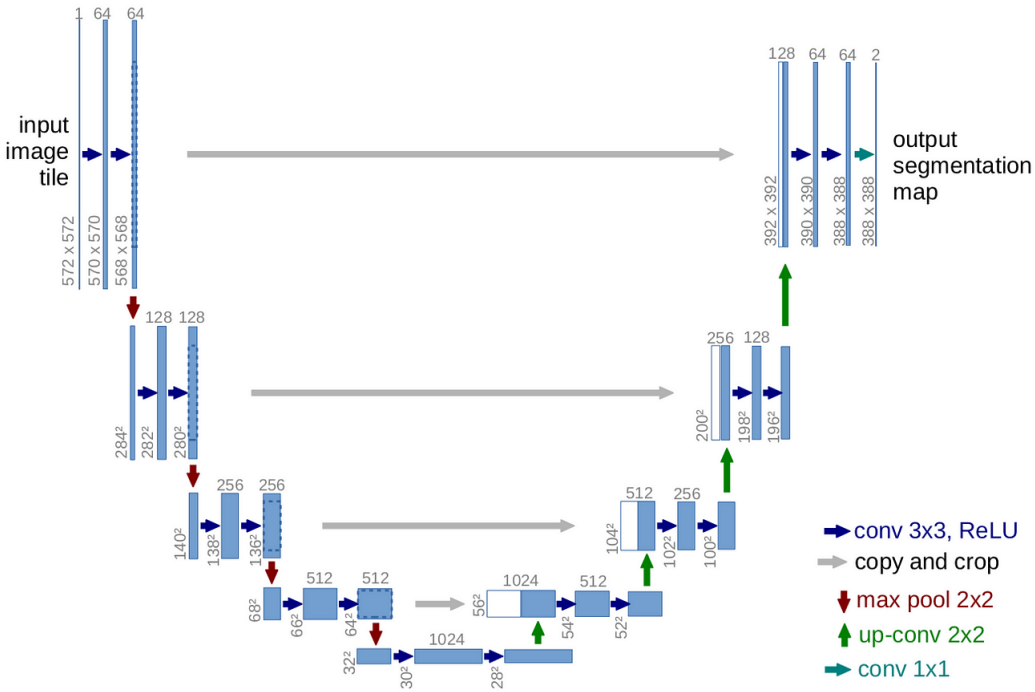

FIGURE 2.8 – U-Net architecture.[52]

Their proprocessing consists of applying a Low-pass filter, then transforming the signals into grayscale images and training the ***U-Net*** model on these images (see figure 2.9).

Authors stated that this method of using ***U-Net*** architecture to purify EEG signals from EOG artifacts, gave precise results of Average Mean Squared Error of **0.0005**, thus the accurate results of the powerful ***U-Net*** architecture.

In another study, Authors in [33] used *heuristic-based convolutional neural network* for artifact removal, and a benchmark dataset was used to evaluate the work, Which is ECG-ID dataset that can be found

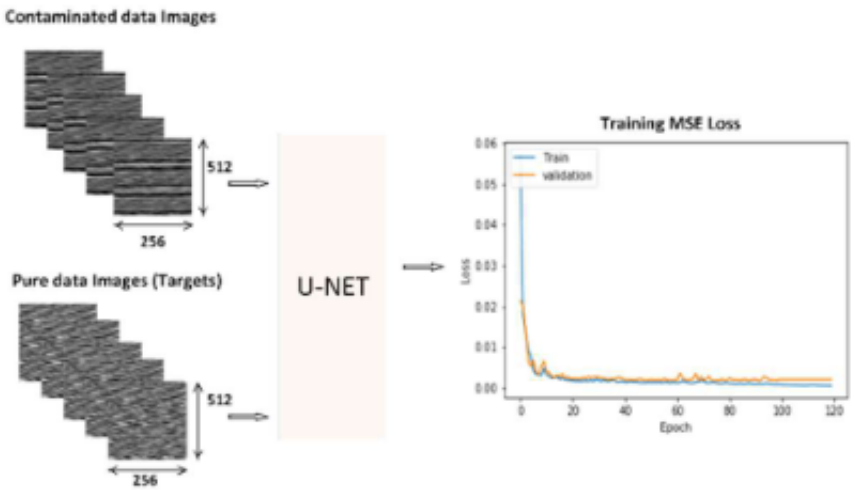

FIGURE 2.9 – U-Net training on gray scale images, evaluation metric is Mean Squared Error (MSE).[32]

in Physio-net platform [1], The model architecture is pretty straight-forward 2 1D convolutional layers, followed with a Fully connected layer, by the end the clean EEG is extracted (See figure 2.10). Authors stated that their model outperformed other state of the art method in SNR, RMSE scores.

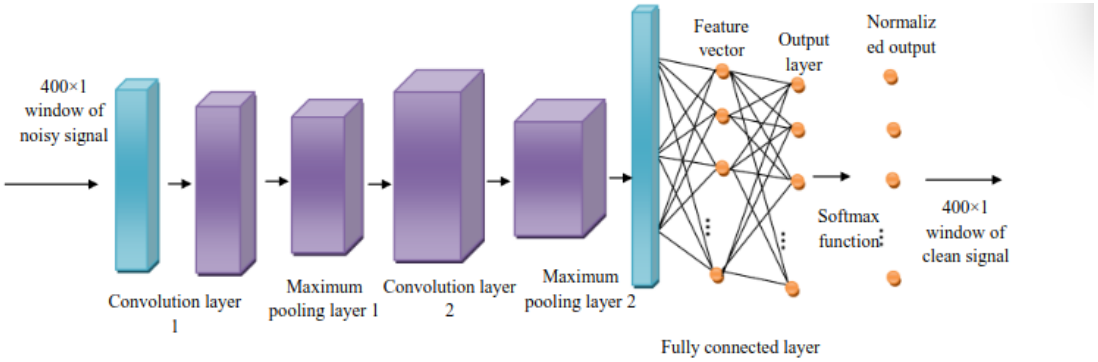

FIGURE 2.10 – Proposed architecture for EEG artifact removal [33]

We looked at how to remove unwanted signals from brain waves (EEG). Techniques like ICA and CCA are like super sorters, separating the important brain activity from things like muscle movements and blinks.

Table 2.1 summarizes the state of the art and provides the advantages and limitations for each method.

TABLE 2.1 – Comparison between the literature reviews.

Authors	**Used Method**	**Advantages**	**Limitations**
Delorme et al. [23] 2006	Independant Component Analysis (ICA)	No prior knowledge of the artifact's characteristics, versatile tool for removing various types of artifacts, such as muscle contractions or eye movements.	Dependence on statistical assumptions.
J.Zheng et al. [36] 2010	Canonical Correlation Analysis (CCA)	Outperforms ICA in EMG Cancellation	CCA is based on the assumption that the underlying sources are mutually uncorrelated while maximally autocorrelated.
Kim et al. [13] 2016	Independant Vector Analysis (IVA)	IVA employs both HOS and the SOS dependence across multiple data sets for jointly achieving independent decomposition of multiple data sets.	Dependancy on Datasets and statistical assumptions
Huang et al. [50] 2009	Ensemble Empirical Mode Decomposition (EEMD)	data-driven and adaptable, effective in removing artifacts with non-stationary characteristics, such as muscle contractions or eye blinks, which can be challenging for traditional filtering methods.	Computationally expensive, Identifying which IMFs contain artifacts and which contain brain activity can be subjective and require some expertise.
Bogdan et al. [35] 2010	EEMD-ICA	Statistically separates the sources and decomposes the signal into intrinsic components which could be robust to non-stationary signals	Computational Complexity, Parameter Tuning, Limited Research.
Najmeh et al. [33] 2020	Deep Learning (DL)	Deep learning models can automatically learn complex features that differentiate brain signals from artifacts	Data Dependency, and computationally expensive.

2.3 PPG Artifact removal

2.3.1 Discrete Wavelet Transform (DWT)

A discrete wavelet transform (DWT) is a transform that decomposes a given signal into a number of sets, where each set is a time series of coefficients describing the time evolution of the signal in the corresponding frequency band. [6]

Unlike the Fourier Transform which uses sine waves, DWT uses wavelets - brief oscillating functions that start and end at zero. These wavelets come in various shapes and sizes, allowing for analyzing various frequency ranges with good time resolution. The signal is passed through filters resembling scaled and stretched versions of the chosen wavelet .e.g *see equation Daubechies wavelet function*. This process decomposes the signal into two parts :

- **Approximation Coefficients** : Capture the overall low-frequency trend of the signal, representing the *big picture*.
- **Detail Coefficients** : Contain the high-frequency information, capturing rapid changes or specific features within the signal.

$$\Psi(t) = (1+\sqrt{2})\left((\sqrt{2}+1)\sin(t) - \cos(t)\right), \quad 0 \le t \le \pi/2 \qquad \text{(Daubechies wavelet function)}$$

This equation defines the shape of the Daubechies wavelet function ($\Psi(t)$) based on time (t). Daubechies wavelets have a whole familly of different orders based on the Length of the filter Vanishing moments or Regularity. see Fig 2.11.

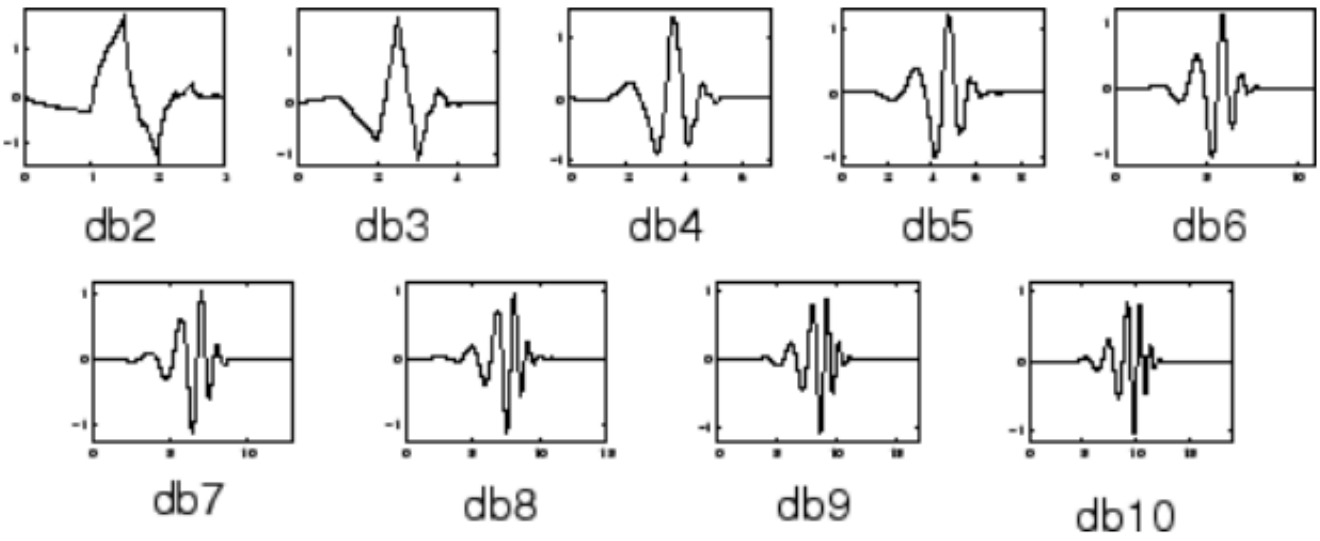

FIGURE 2.11 – Daubechies Wavelet Families based on their order. [7]

Similar to wavelets, scaling functions are used in DWT ater the signal is decomposed the reconstruction using the the scaling function 1.

$$\Phi(t) = \left(\left(1+\sqrt{2}\right)\cos(t) + \left(\sqrt{2}-1\right)\sin(t)\right)^2, \quad 0 \le t \le \pi. \tag{1}$$

A study investigated the use of DWT for denoising PPG signals acquired from the fingertip, specifically to address motion artifact contamination [16]. Clean up PPG signals was collected from 40 healthy volunteers. Authors in [16] created artificial noise by adding motion data to real PPG readings. This noisy data went through wavelet decomposition to separate different frequencies. Then, soft thresholding was applied at each frequency level to remove the noise. The authors tested different approaches within this process (wavelet functions and thresholding methods) to find the best way to remove the motion interference from the PPG signals. 2.12

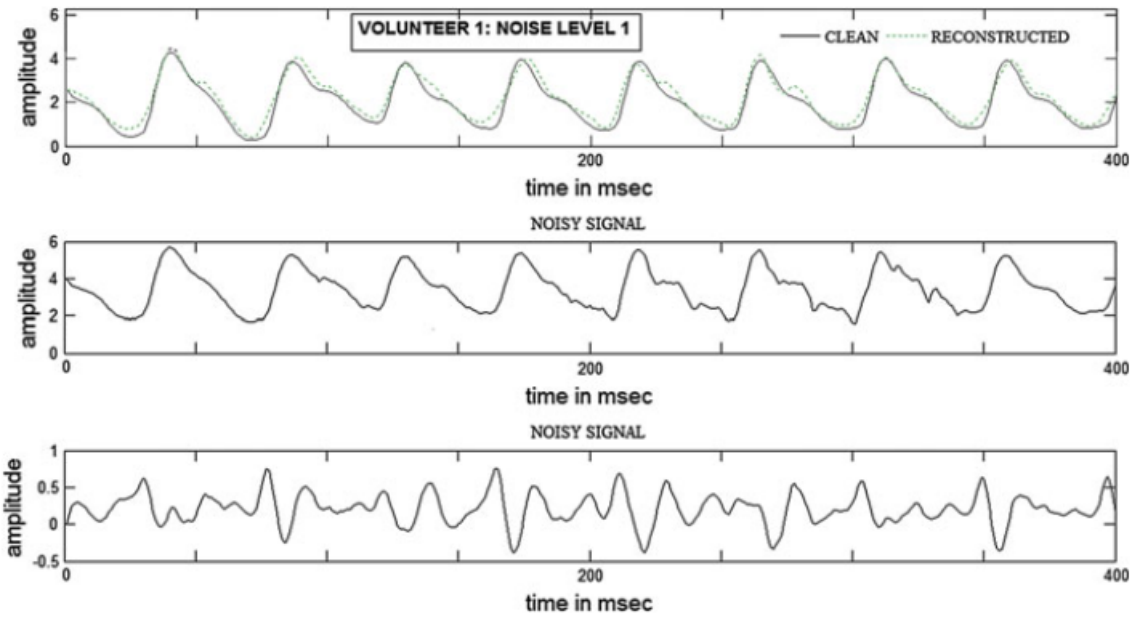

FIGURE 2.12 – Subjective assessment of denoising performance [16]

2.3.2 Statistical approaches

The simplest approach was done by authors in [26], where they used only statistical parameters of the PPG signal to detect and cut out signal parts contaminated with Movement Artifacts (MAs) [40] [see Fig 2.13].

Prior to the analysis, the algorithm performs a filtering step. This step employs a band-pass filter tuned to capture frequencies within the 0.5 to 6Hz band. This specific range is crucial as it encompasses the essential frequencies for detecting heart rate. Afterwards it is segmented based on the signal period and from the segmented signal the standard deviation, skewness, and kurtosis is calculated using the following equations :(Standard Deviation 2), Kurtosis :*3, Skewness : 4)*

$$\sigma = \sqrt{\frac{1}{N}\sum_{i=1}^{N}(x_i - \overline{x})^2} \tag{2}$$

$$K = \frac{\frac{1}{N}\sum_{i=1}^{N}(x_i - \overline{x})^4}{\sigma^4} \tag{3}$$

$$Sk = \frac{\frac{1}{N}\sum_{i=1}^{N}(x_i - \overline{x})^3}{\sigma^3} \tag{4}$$

If there's no movement while recording, the different calculations we do on the data, like how pointy or lopsided it is (kurtosis and skewness), and how spread out it is (standard deviation), will be very similar for each cycle. This means the data is consistent throughout. Movement significantly alters the PPG signal's amplitude. This, in turn, causes the calculated statistics (kurtosis, skewness, and standard deviation) to exceed predefined thresholds, flagging the signal as corrupted. Consequently, these corrupted segments are removed from the original recording, leaving only the clean data behind.[40].

To assess the performance authors stated that the method was tested with 10 healthy subjects who had to perform four different tasks : (i) no movement, (ii) finger movement, (iii) wrist movement, and (iv) elbow movement.(see figure 2.14)

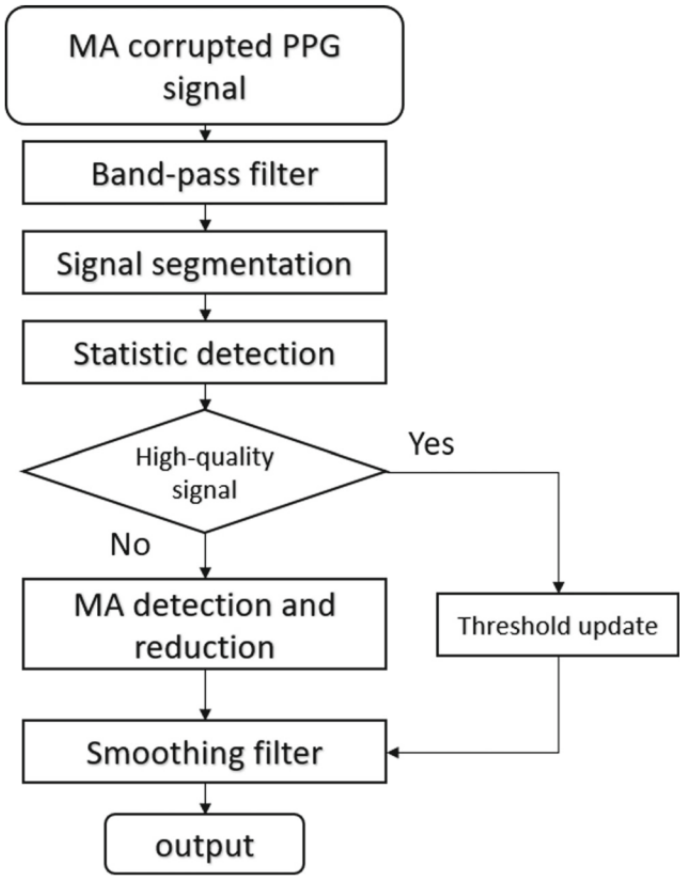

FIGURE 2.13 – Proposed methodology for statistical approach [26]

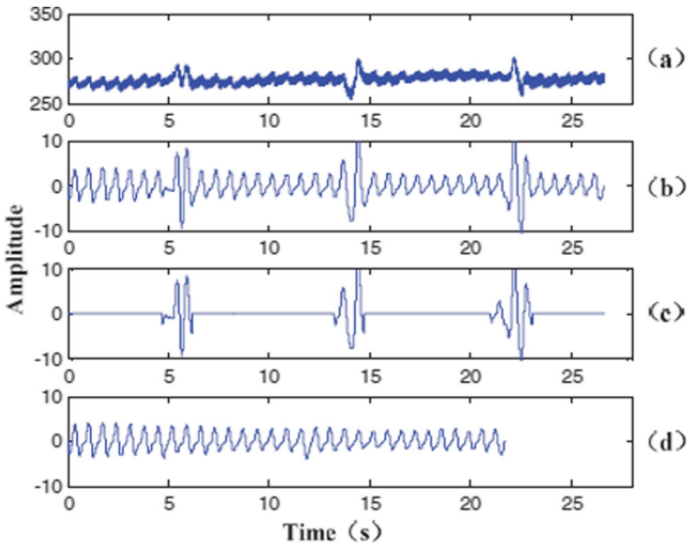

FIGURE 2.14 – **a** Original PPG signal, **b** PPG after pre-processing, **c** detected movement, **d** cut-out algorithm applied [26]

2.3.3 Deep Learning approaches

Recent advancement in the Deep Learning field as mentionned in the last section, were seen in purifying PPG signals from **Mouvements artifacts**. For instance authors in [9] used *CycleGAN* for Artifact removal on real data merged with generated accelerometer data while putting *BIDMC Dataset* [39] as cleaned dataset to asses the perfomance of their algorithm that we will discuss by next.

Data Description : Authors carried out laboratory-based experiments to gather accelerometer data for creating noisy PPG signals. Each of these experiments lasted 27 minutes. A total of 33 participants took part in these experiments, with ages ranging from 20 to 62. Of these participants, 17 were male and 16 were female. During each experiment, participants were instructed to engage in specific activities while their accelerometer data were recorded using an Empatica E. more details could be found in the same paper[9].

Flowchart of the artifact removal model :

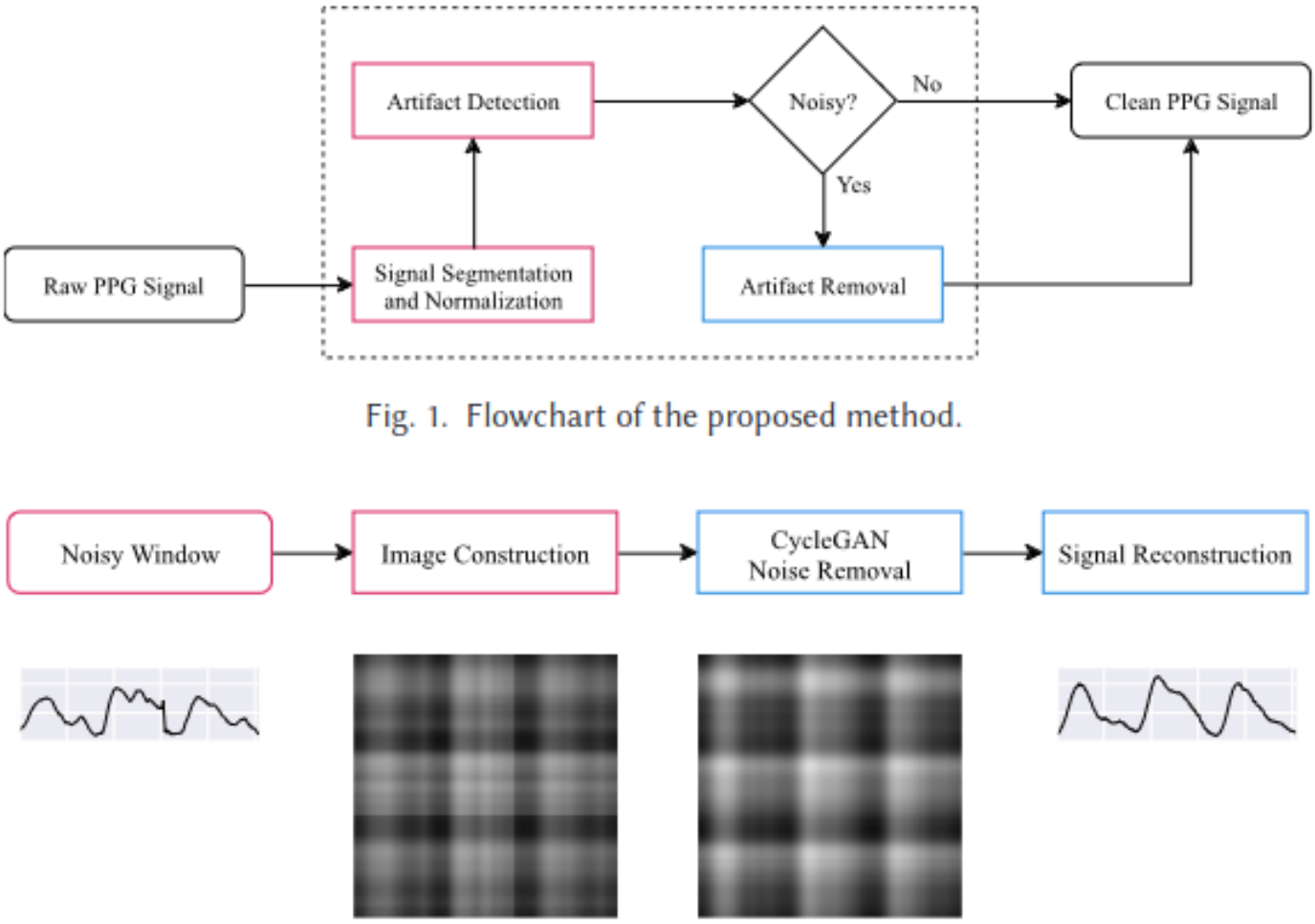

FIGURE 2.15 – Flowchart of artifact removal [9]

This Generetaed accelerometer data were added by next to ***BIDMC*** PPG signals datasets for the model training (see figure 2.15). *The desciption of the model will be discussed in the depth, as we will be imlpemeting the same model for different tasks later on.*

Raw PPG signals enters a block where the signal is going to be segmented into smaller windows to process them and detect if the signal is noisy or not using a deep CNN network, if the signal is noisy and it will be sent to the artifact removal model which is the ***CycleGAN*** model to remove the artifacts, if not the window wil be ignored.

PPG signal purification is an active area with both statistical and deep learning approaches showing promise. Statistical methods offer a solid foundation for real-time applications, while deep learning pushes the boundaries of noise removal and feature extraction. The best choice depends on your needs, with future advancements likely to involve hybrid methods and improved interpretability in deep learning models.

Table 2.2 summarizes the existing methods with their according papers, stating some of their advatanges and limitations in real world problems.

TABLE 2.2 – Comparison between the literature reviews.

Paper	**Method**	**Advantages**	**Limitations**
Biswas et al. [16] 2018	Discrete wavelet transform	DWT decomposes the PPG signal into different frequency bands using wavelet functions. This allows for targeted removal of artifacts that reside in specific frequency ranges, such as power line noise or muscle movement artifacts, while preserving the heart rate information typically found in lower frequencies.	DWT might not completely eliminate all artifacts, especially if they overlap significantly in frequency with the heart rate signal, computationally expensive.
Hanyu et al. [26] 2017	Statistical approaches	remove various noise sources that corrupt the PPG signal, such as motion artifacts, baseline wander, and power line interference, computationally efficient	Statistical methods often rely on assumptions about the noise distribution. If these assumptions are violated, the filtering performance can degrade, Overaggressive noise removal techniques might inadvertently distort the underlying PPG signal.
Zargari et al. [9] 2023	Deep Leaning (CycleGAN)	Deep learning models can learn complex relationships between the PPG signal and various noise sources, and eliminates the need for manual feature selection, which can be a challenge in traditional approaches.	Deep learning models are susceptible to overfitting, where they learn the training data too well and perform poorly on unseen data, computationally expensive and resource-intensive.

2.4 Conclusion

At the end of this chapter, we have explored the various existing approaches for artifacts removal while analyzing neuro-physiological signals

We should mention that *Methods of purifying EEG signals won't work on purifying PPG signals and viceversa* due to several points :

Physiological origin of signals :

- EEG (Electroencephalography) : Measures electrical activity in the brain. EEG signals are weak and susceptible to various electrical interferences from muscles, eyes, and power lines.
- PPG (Photoplethysmography) : Measures changes in blood volume in the microcirculation using light. PPG signals are affected by motion artifacts, breathing patterns, and ambient light variations.

Noise characteristics :

- EEG : Prone to high-frequency noise from muscle activity (EMG) and power line interference (50/60 Hz).
- PPG : Primarily affected by low-frequency noise due to motion artifacts (breathing, body movement) and baseline wander caused by slow blood volume changes.

Signal processing techniques :

- EEG filtering : Often involves notch filters to remove power line interference and high-pass filters to eliminate slow baseline wander.
- PPG filtering : Employs low-pass filters to suppress high-frequency noise from muscle activity and baseline wander correction algorithms to address low-frequency drifts.

Finally, the filtering techniques target specific noise sources based on the signal's origin and characteristics. EEG methods focus on removing high-frequency electrical interference, while PPG methods target low-frequency motion artifacts and baseline variations.

While some general signal processing techniques might overlap (e.g., filtering fundamentals), the specific methods need to be tailored to the unique characteristics and noise sources of each physiological signal.

In the next chapter we investigate the performance of the algorithms. and propose a new developments and approaches in this field.

Chapitre 3

Methodology

3.1 Introduction

This section outlines the methodology employed for artifact removal in biomedical signals, focusing on the use of CycleGAN and deep Convolutional Neural Networks (CNN). These advanced deep learning techniques were chosen for their ability to effectively learn and mitigate complex noise patterns inherent in Electroencephalography (EEG) and Photoplethysmogram (PPG) signals.

3.2 Deep Convolutional neural networks

This section dives into the powerful world of deep convolutional neural networks (CNNs) and explores their remarkable ability to remove artifacts from biomedical signals. We'll see how these intelligent algorithms can learn to distinguish the true signal from unwanted noise, leading to cleaner data and more accurate diagnoses.

3.2.1 Model Architecture

Our model consists of different CNN residual blocks that will encorporate between each other to extract the important information and remove all kinds of artifacts. Please see Fig.3.1

The first block which is the blue one, consists of **4** 1D CNN layers with different '**Input channels shape**', '**Output channels shape**', '**kernel size**', '**Padding size**', same as for the second block which is the green one, it consists of **4** 1D CNN layers except for this time the **Input Channels shape** is **20**, the interesting part about this block is that is a residual block, which keep extracting features and rotating on it self 3 times to ensure the deep extraction.

The squeezing block which is the rose one, consists of **1** 1D CNN layer to compress the 20 channels into 1 channel. For this time the **Blue**, **Green** and **red** combine and the output is passed 3 times as a bigger residual block.

Afterwards, the output of these residual blocks, get activated with **Sigmoid** function, a **squeezing 1D CNN** layer. As a final touch the output passed by the first 3 blocks 'Blue, Green, Red' and this is our final output.

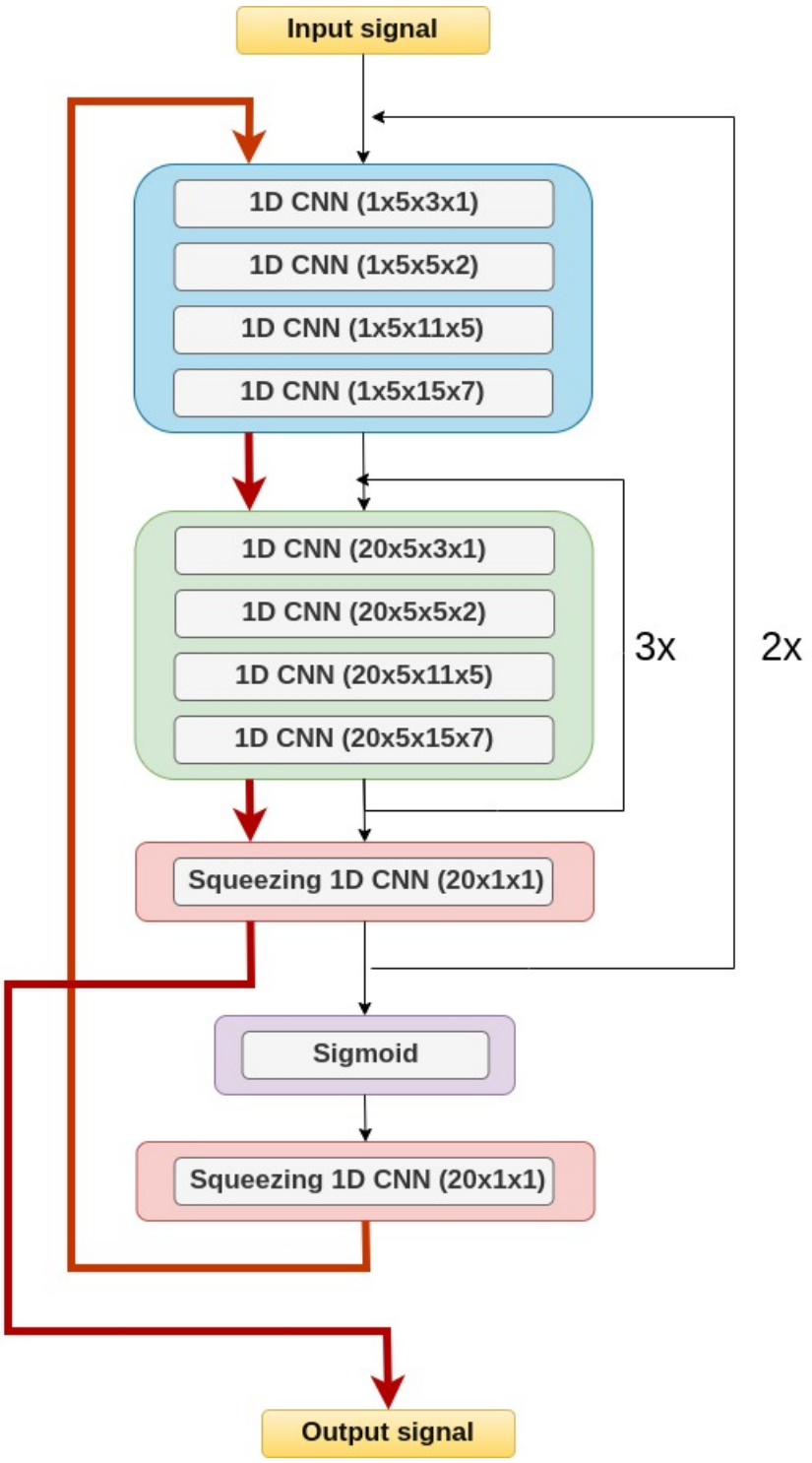

FIGURE 3.1 – Proposed Model Architecture consisting of 3 main blocks Blue, Green, Rose

3.2.2 Learning Process

To train the model accurately, we utilize the mean squared error (MSE) function (represented by the loss function 5) to assess the difference between the restored signal and the original clean one. A technique called gradient descent is then employed to minimize this error during the training process, effectively removing noise from the signal.

$$L_{MSE} = \frac{1}{N}\sum_{i=1}^{N} ||\bar{x}_i - \hat{x}_i||_2^2 \tag{5}$$

We will be using **Adam optimizer**, to optimize models parameters and also to make sure the good convergence of the model. Also a **Learning rate** = 0.001 will be applied for the model.

3.3 CycleGAN

While deep convolutional neural networks excel at denoising, let's explore another intriguing deep learning technique : CycleGAN. Unlike CNNs trained for specific noise patterns, CycleGAN offers a unique approach to artifact removal in biomedical signals. This section delves into CycleGAN's capabilities and how it could potentially revolutionize biomedical data cleaning.

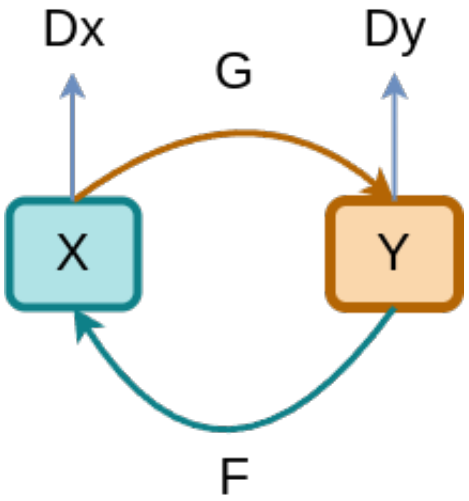

FIGURE 3.2 – CycleGAN main architecture, G and F are the mapping functions, D_x and D_y are the descriminators, X and Y are the spaces.

3.3.1 CycleGAN Architecture

CycleGAN [53], mainly consists of two mapping functions that are basically two generators, let's name them for instance G and H, $G : X \rightarrow Y$ tries to generate similar images to the ones are in space Y, then $H : Y \rightarrow X$ tries to reconstruct back the original image in space X, since there is generation within spaces, we introduce two discriminators alongside the the mapping function named D_x and D_y, to determine whether the generated images are **Real** or **Fake**. for this there is a cycle between the two generators, Thus the model was named for this cycle and the two GANs ***CycleGAN*** !. (See figure 3.2)

3.3.1.1 Generators Architecture

Both Mapping function 'Generators' have the same architecture in CycleGAN architecture 3.3

The **Generator** architecture begins with a **Reflection Pad** which is basically a mirror for the image meaning that the input image will be concatenated with its own image, followed by a **Convolution Layer**, **Instance Normalization** followed by a **ReLU Activation**. Next there is a **Downsampling block** for reducing the input resolution which will be happening for 2 consecutive times, Next is the **Residual block** to extract meaningful features which will be occuring for 9 consecutive times. the **Residual block** is straightforward, it begins with a **Reflection Pad** then **Convolutional Layer** followed a **Instance Normalization** activated with a **ReLU function**, then the first 3 layers occur again.

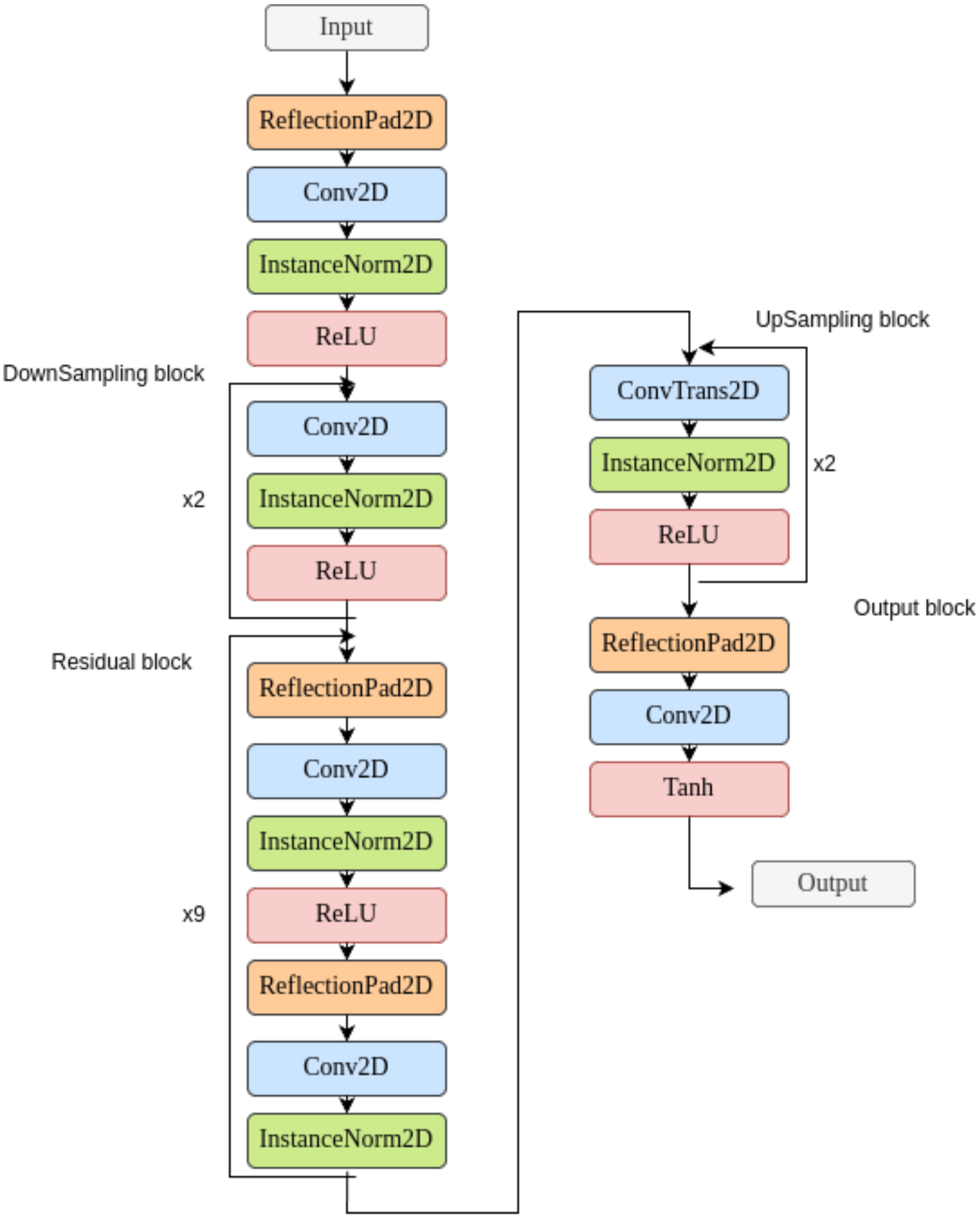

FIGURE 3.3 – Mapping Function '*Generator architecture*'

Finally, a **UpSampling block** to reconstruct back the generated tensors into an actual image by passing by a **Transpose Convolutional layer**, **Instance Normalization** and a **ReLU function**, this will be happening 2 consecutive times. And an Output Block for the generated image using the Mapping function. 3.3

3.3.1.2 Discriminators Architecture

Both Discriminators have the same architecture in CycleGAN architecture 3.4

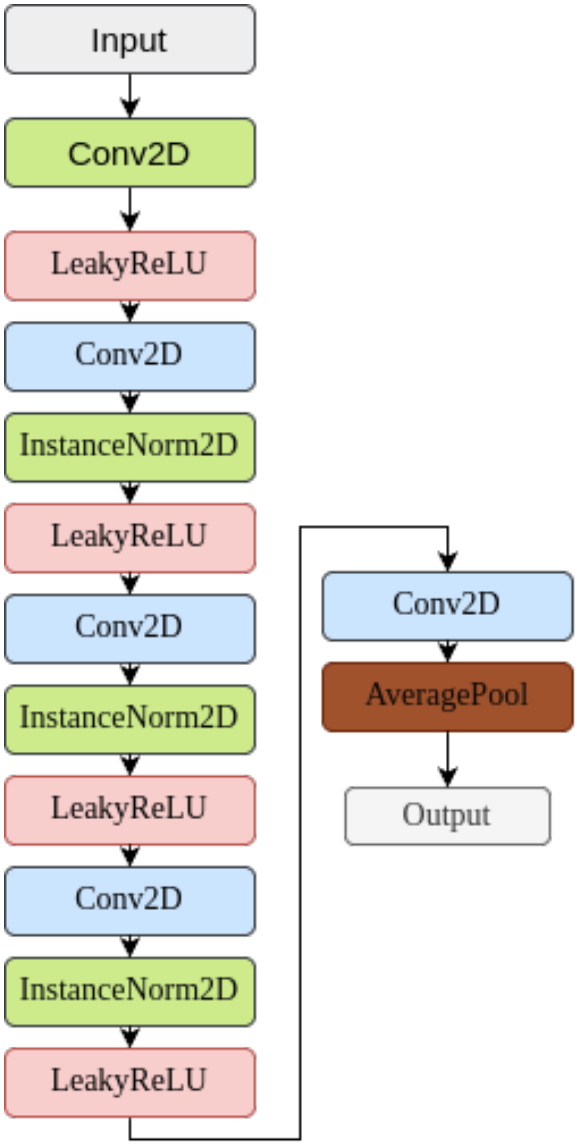

FIGURE 3.4 – Discriminators Architecture

3.3.2 Learning process

CycleGAN training is somehow special since it utilizes two pairs of networks : generators and discriminators. Each generator transforms data from one domain into the other, while the discriminators assess the realism of these generated images. However, this process doesn't guarantee perfectly mapped outputs. To address this, CycleGAN incorporates another loss called cycle consistency loss. Imagine feeding the output of the first generator back into the second one. Ideally, this should result in an output close to the original input data (and vice versa). By incorporating this loss function that measures this discrepancy, CycleGAN steers the generation process towards achieving true data translation.

Adversarial Loss is applied for both of the two mapping functions $G : X \rightarrow Y$ and $F : Y \rightarrow X$ The objective of the mapping function G as a generator and its discriminator D is expressed as below :

$$L_{GAN}(G, D, X, Y) = E[log(D(y))] + E[log(1 - D(G(x))].$$

Where the mapping function **G** takes a sample from *Space X* (e.g. Noisy PPG signal) attempting to generate new data that is similar to *Space Y* (e.g. clean PPG signal). Whilst that **D(y)** aims to determines if the reconstructed image (clean PPG signal) is actually clean and real or not. This Adversarial Loss is defined for both of the mapping Functions **G** and **F**.

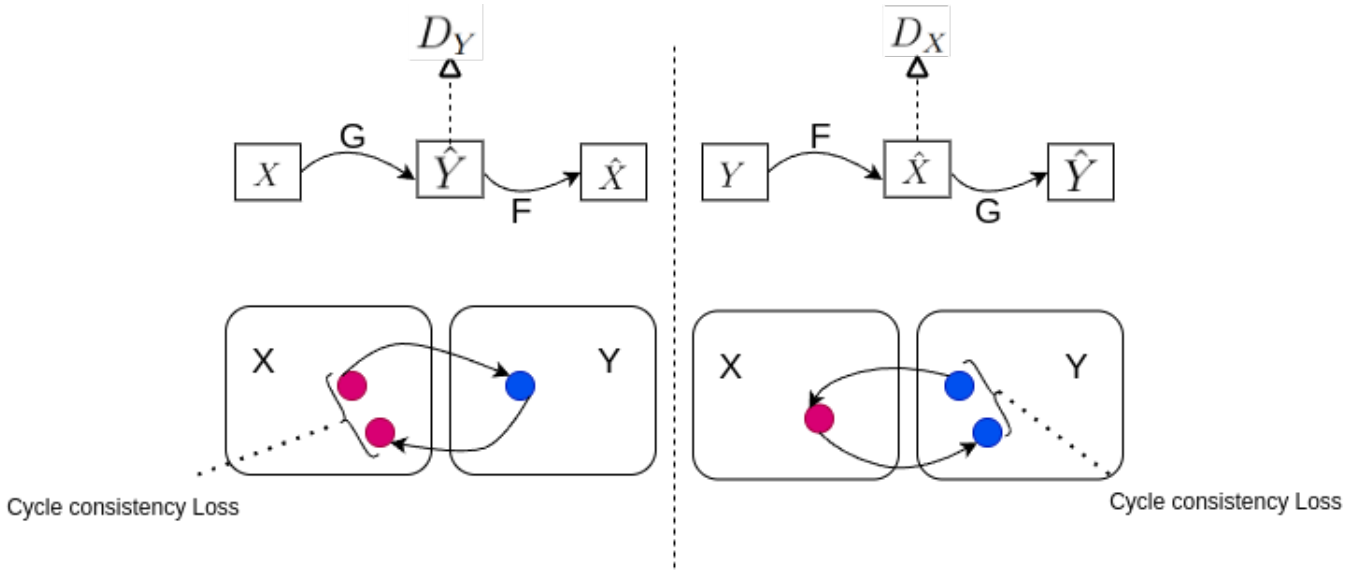

FIGURE 3.5 – Forward and Backward consistency losses, and the descrimination losses.

In this case of study, Adversarial Losses alone cannot guarantee that the learned mapping function can map an input to the desired output (e.g purifying PPG signal), authors in [53] discovered that the learned mapping functions (G and F) need to be **Cycle-consistent**, this means that the translation cycle should be able to translate back the input from space X to the original image X as $X \rightarrow G(X) \rightarrow F(G(X)) \approx X$, this is called **Forward cycle consistency**. Similarly for **Backward cycle consistency** is defined as $Y \rightarrow F(Y) \rightarrow G(F(X)) \approx Y$ (See figure 3.5), thus **Cycle Consistency** loss function is defined as :

$$L_{Cycle}(G, F) = ||F(G(X)) - X||_1 + ||G(F(X)) - Y||_1.$$

Therefore the final objective of **CycleGAN** (Loss function) is defined as :

$$L(G, F, D_X, D_Y) = L_{GAN}(G, D_Y, X, Y) + L_{GAN}(F, D_X, Y, X) + \lambda L_{Cycle}(G, F).$$

Where λ controls the relative importance of the **Cycle consistency loss**, whilst mapping function **G** tries to minimize the Loss, and an adversary D attempts to maximize it, therefore our model aims to solve :

$$G^*, F^* = argmin L(G, F, D_X, D_Y).$$

3.4 Evaluation metrics

Various metrics are employed to qualitatively assess network performance, encompassing aspects such as network convergence, relative root mean squared error, and correlation coefficient.

Network Convergence measurement in training a network can be initially judged by how well it converges. Convergence tells us a lot about how the network learns and its ability to perform well on unseen data (generalization ability).

RMSE, or Root Mean Squared Error, is a metric used to assess how accurate a predictive model is. It calculates the average magnitude of the difference between the predicted values and the actual values. By squaring these differences, giving more weight to larger errors, then averaging and taking the square root, RMSE provides a single score.

Generally, a lower RMSE indicates a better fit between the model's predictions and the real data.

Signal-to-noise ration (SNR) Signal-to-noise ratio (SNR or S/N) is a measure used in science and engineering that compares the level of a desired signal to the level of background noise. SNR is defined as the ratio of signal power to noise power, often expressed in decibels. A ratio higher than $1:1$ (greater than 0 dB) indicates more signal than noise.

$$SNR = \frac{P_{Signal}}{P_{Noise}},$$

where P is the average power. Both signal and noise powers must be measured at the same or equivalent points in the system, and within the same system bandwidth. [49]

3.5 Conclusion

In this chapter, we meticulously detailed the framework employed for purifying neurophysiological signals using advanced algorithms. We introduced the architecture and mechanisms of deep convolutional neural networks (CNNs) and discussed their application in signal processing. Additionally, we presented CycleGAN, emphasizing its role in generating high-quality signal transformations. We also outlined the evaluation metrics, including root mean squared error, model convergence, and signal-to-noise ratio (SNR), essential for assessing the performance of the proposed methods.

Transitioning to the next phase of the project, the upcoming chapter will delve into the experimental results. We will analyze the performance of the discussed algorithms, providing comprehensive insights into their effectiveness in EEG and PPG signals purification. and propose a new contribution in removing artifacts from EEG signals using CycleGANs, and asses its performance in contrast to the state of the art algorithms.

Chapitre 4

Purifying EEG and PPG signals

4.1 Introduction

Getting clear readings from our bodies is crucial for doctors to understand our health. This chapter explores how deep learning can help remove unwanted "noise" from two important signals : brain waves (EEG) and heart rate/oxygen levels (PPG).

The following sections we will explore two innovative approaches, each tailored to address artifacts in a specific type of biomedical signal.

4.2 Deep CNN for EEG artifact removal

Electroencephalogram (EEG) signals offer a window into brain activity. However, artifacts like muscle movements and eye blinks can contaminate these signals. This section will introduce the application of Deep CNNs for EEG artifact removal. These powerful networks can learn complex patterns within the EEG data, effectively separating the true brain signal from the artifactual noise.

Traditional methods for removing artifacts from EEG signals often fall short when dealing with the complexity of real-world data. Deep CNNs emerge as a powerful alternative motivated by this very need. EEG recordings are susceptible to various interferences, making it difficult to isolate the brain's electrical activity. Deep CNNs aim to surpass existing techniques by learning intricate patterns within the data. This allows them to distinguish true brain signals from artifacts with greater precision. The ultimate goal is to develop CNN models that work across diverse datasets and potentially even process data in real-time. This would significantly streamline EEG analysis and pave the way for cleaner, more reliable data for applications like epilepsy diagnosis and brain research.

CNNs have the potential to be optimized for real-time processing, enabling artifact removal during data acquisition. This would be particularly valuable in applications like Brain-Computer Interfaces (BCIs) where immediate signal processing is crucial. For that we will be using the model presented in section 3.2.

4.2.1 EEGdenoiseNet Dataset

EEGdenoiseNet Dataset is a publicly available benchmark dataset used to assess different algorithms performance on EEG dataset.

4.2.1.1 Data Collection

The creators of this dataset [51] that consists of 3 different types of signals **EEG**, **EOG**, **EMG** stated that it was mainly constructed using available datasets. Then this dataset was preprocessed and segmented into epochs of 2 seconds. Afterwards the epochs are scaled to have the same variance then a visual checking is performed to ensure the quality of this epochs and if its clean and ready to test.

This data was collected and acquired from open access archives and was used in previous studies. Those studies were revised and approved by respective local ethical committees and followed the Helsinki Declaration 1975, revised in 2000.

For the EEG epochs (Figure 4.1a), They used an EEG dataset for motor imaginary brain computer interface. The EEG dataset consists of 64-channel (with international 10-10 system, and sampled at 512 Hz) EEG both for imaginary and real movement conditions of left and right hand. The data were band-pass filtered between 1 to 80 Hz and notched at powerline frequency, followed by re-sampling to 256 Hz ; then the 64-channel signals were processed using ICLabel to attenuate artefacts. Then the EEG signals were segmented into epochs of 2 seconds.

For the ocular artifact epochs (Figure 4.1b), multiple datasets were collected from open-access EEG data. The horizontal and vertical electroculagraphy (EOG) signals of the datasets were band-pass filtered between 0.3 and 10 Hz, followed by re-sampling to 256 Hz ; then the signals were segmented into epochs of 2 seconds.

For the myogenic artifact epochs (Figure 4.1c), a facial surface electromyography (EMG) dataset was used.They chose facial EMG because they are the main sources of myogenic artifacts. The EMG signals were band-pass filtered between 1 to 120 Hz and notched at powerline frequency, followed by re-sampling to 512 Hz ; then the signals were segmented into epochs of 2 seconds.

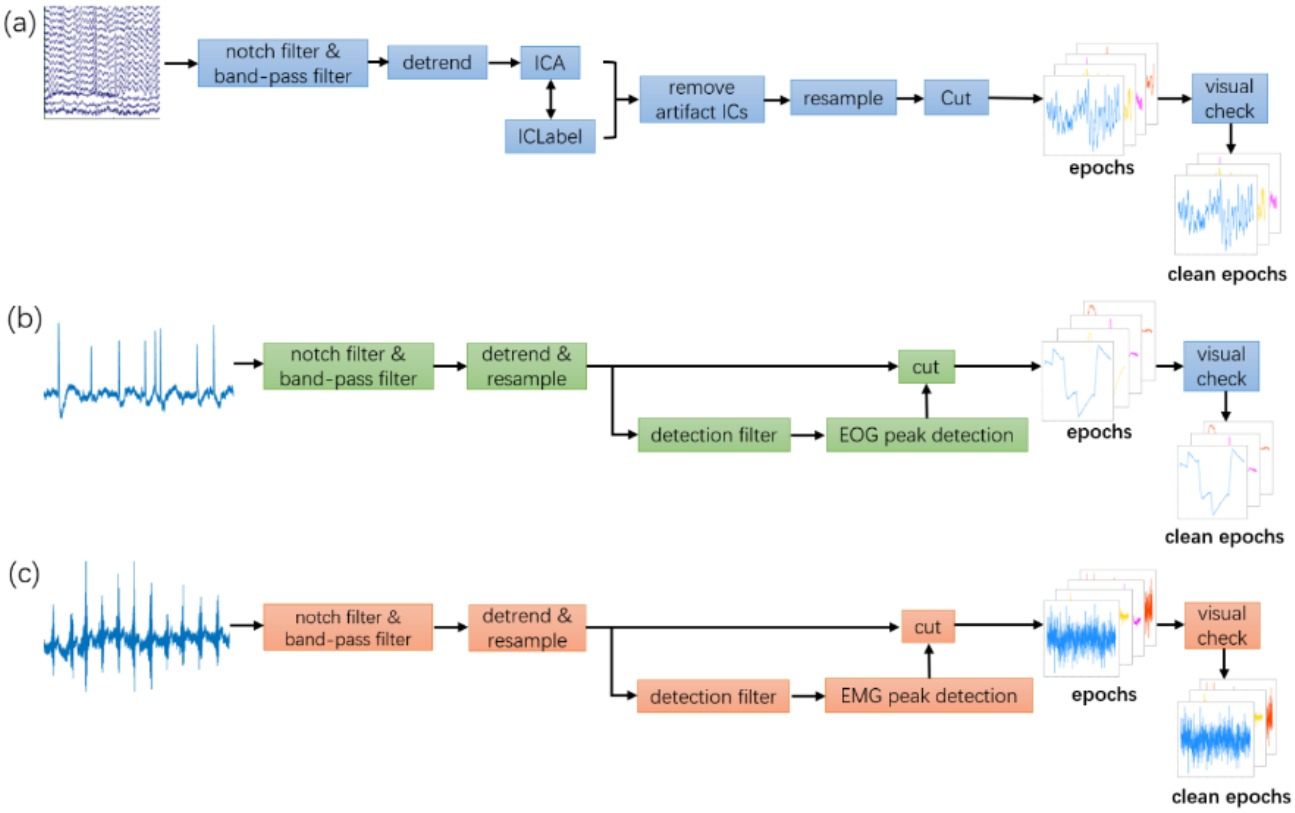

FIGURE 4.1 – The pipeline for obtaining clean EEG, EOG and MEG. [51]

or all the categories, the epochs were standardized by subtracting their mean and dividing by their

standard deviation, and then were visually checked by an expert. Finally they acquired 4514 EEG epochs, 3400 ocular artifact epochs and 5598 myogenic artifact epochs. The epochs for each category were saved separately as Matlab matrix files and Python numpy matrix files to a public data repository.

4.2.1.2 Data Usage

One way to create simulated signals with noise is to combine segments of EEG data (epochs) with segments of EOG or EMG data using the linear Mixing formula 6 :

$$y = x + \lambda.n \tag{6}$$

Where y denotes the mixed signals between **EEG** and **EOG**, or **EEG** and **EMG**. x denotes the clean **EEG** signal, n denotes the artifacts **EMG** or **EOG**, and lastly λ denotes the relative artifact's contribution [51]. Further exampels on the signals **EEG** and it's mixture with both artifacts separately 4.2, 4.3 , 4.4, 4.5

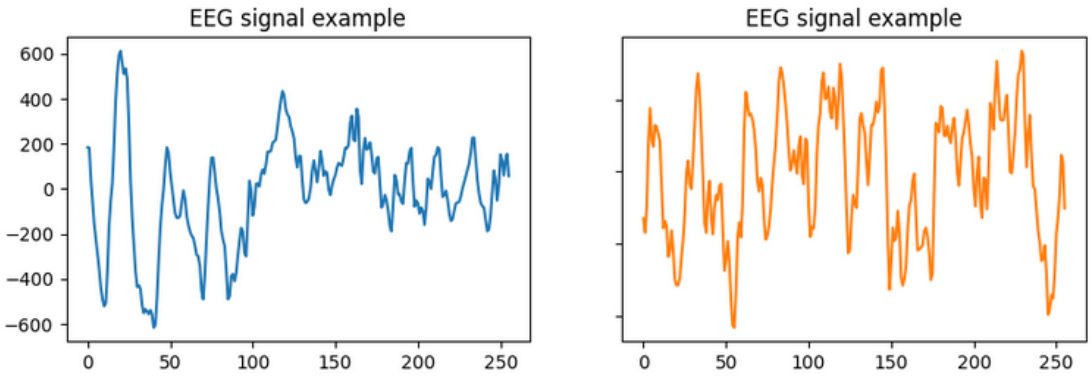

FIGURE 4.2 – examples of EEG signals.

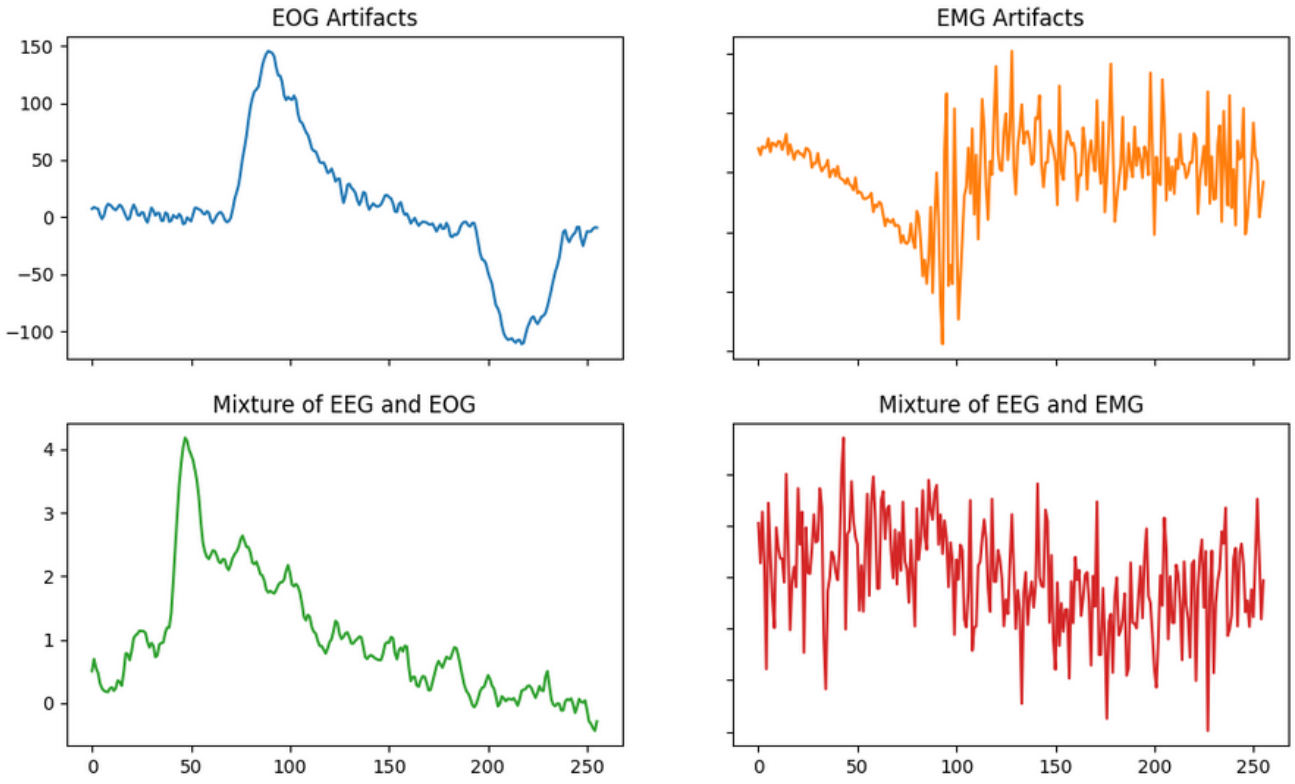

FIGURE 4.3 – Artifacts (EMG, EOG) and their mixtures with EEG.

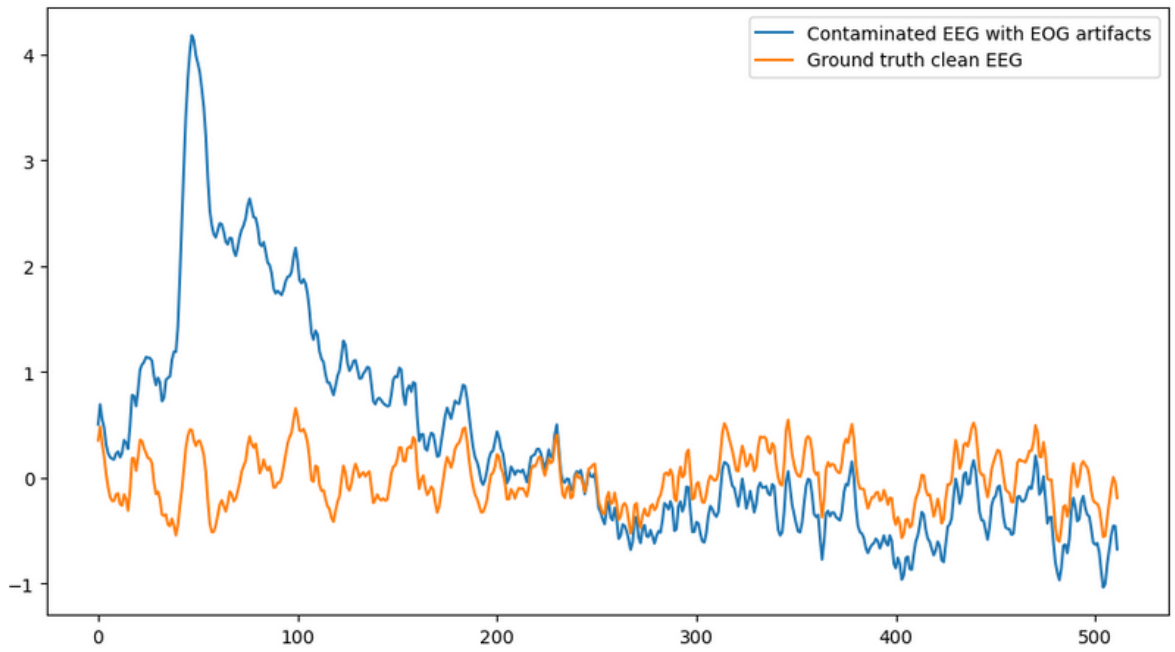

FIGURE 4.4 – EEG mixed with EOG artifacts.

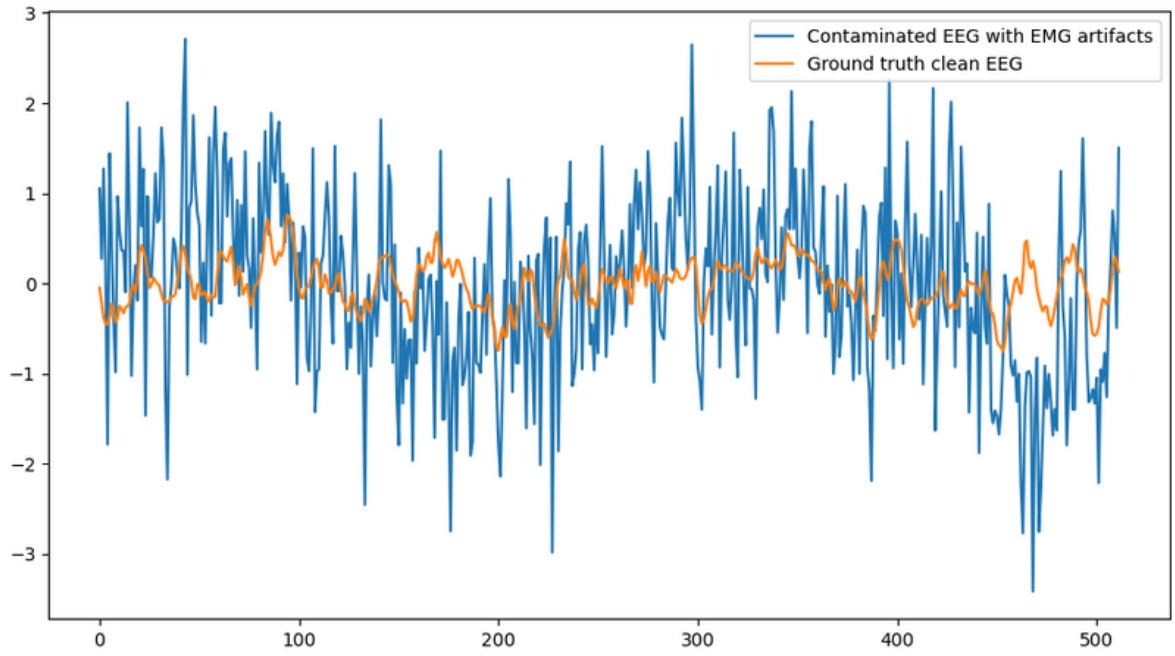

FIGURE 4.5 – EEG mixed with EMG artifacts.

4.2.1.3 Data preparation

The studied dataset consists of 3400 paired segments of EEG data and data containing eye movement artifacts (EOG). The dataset was divided for training and testing purposes, with 3000 pairs used to train the model and 400 pairs kept separate for evaluation. To create the training data, 3000 EEG-EOG pairs were randomly mixed together ten times with 10 different **SNR** levels (-7dB, -6dB, -5dB, -4dB, -3dB, -2dB, -1dB, 0dB, 1dB, 2dB). according to the following **SNR** formula.

$$SNR = 10.log\frac{RMS(x)}{RMS(\lambda.n)}.$$

In which the Root Mean Squared (RMS) value is defines as :

$$RMS(x) = \sqrt{\frac{1}{N}\sum_{i=1}^{N} ||g_i||_2^2},$$

where N denotes the samples count of an epoch g_i and g_i denotes the i^{th} sample of an epoch g. furthermore see Table 4.1 to know more about Training/Test distribution sets.

TABLE 4.1 – Train/Test distribution

Signal type	Number of signals	Signal length
EEG + EMG	60000 Train / 4000 Test	512
EEG + EOG	60000 Train / 4000 Test	512
Training (EEG+EMG | EEG+EOG)	120000 Train / 8000 Test	512

4.2.2 Experimental Results

After applying and following the defined learning process in the previous subsection, the model training and testing loss were as follows 4.6 :

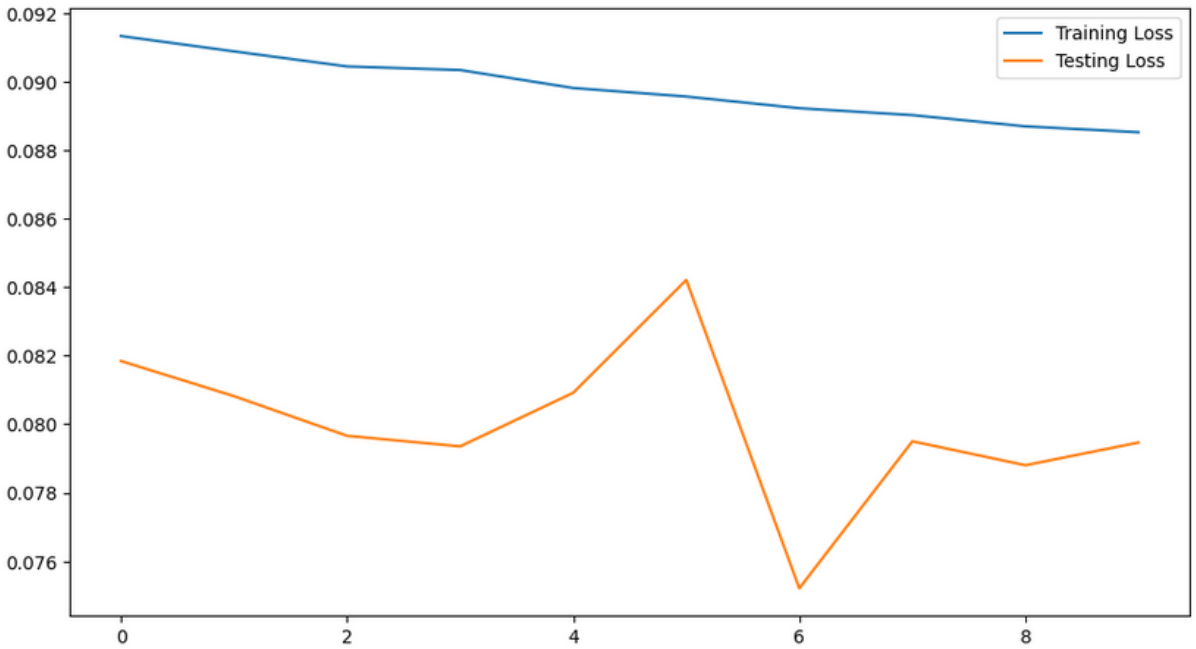

FIGURE 4.6 – Training and Testing loss for the defined model in 3.1.

Training and testing loss are evaluated using the Mean Squared Error as defined in 5, Thus both graphs converge to very low error rate which is approximatley **0.09** for the **training Loss**, and **0.08** for the **testing Loss**.

Due to computational issues, the model was trained only for **10 epochs** as mentionned before in the section 3.2.2.

After saving best model parameters, the model was put again for testing to visualize some noisy signals and an estimation for the cleaned signal.

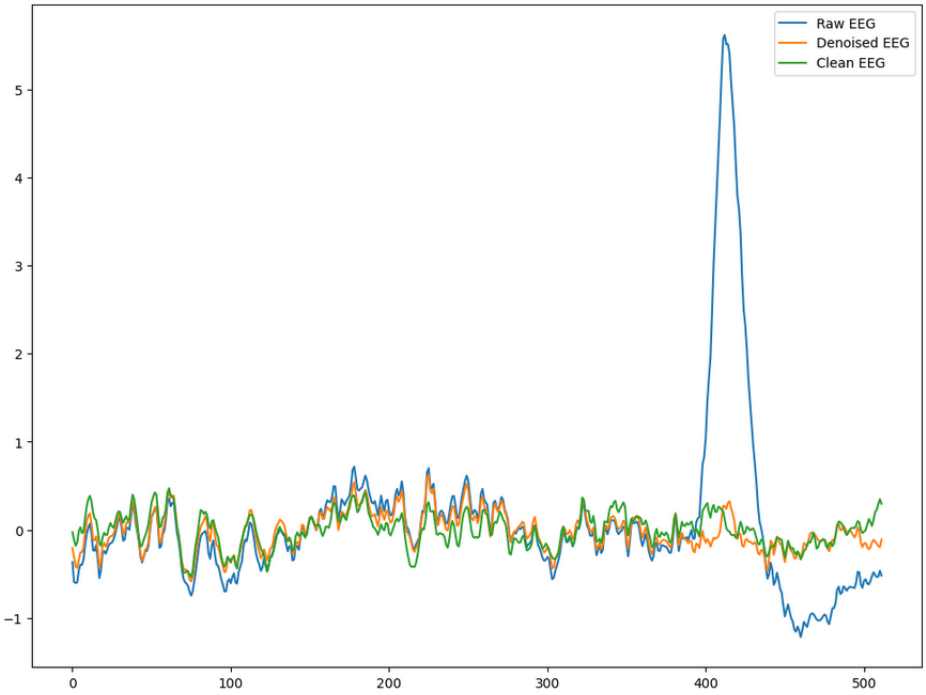

FIGURE 4.7 – Model testing on a contaminated EEG signal with EOG artifacts with, **Blue** is the Raw EEG to be cleaned, **Orange** : The estimated signal, **Green** : Ground truth signal.

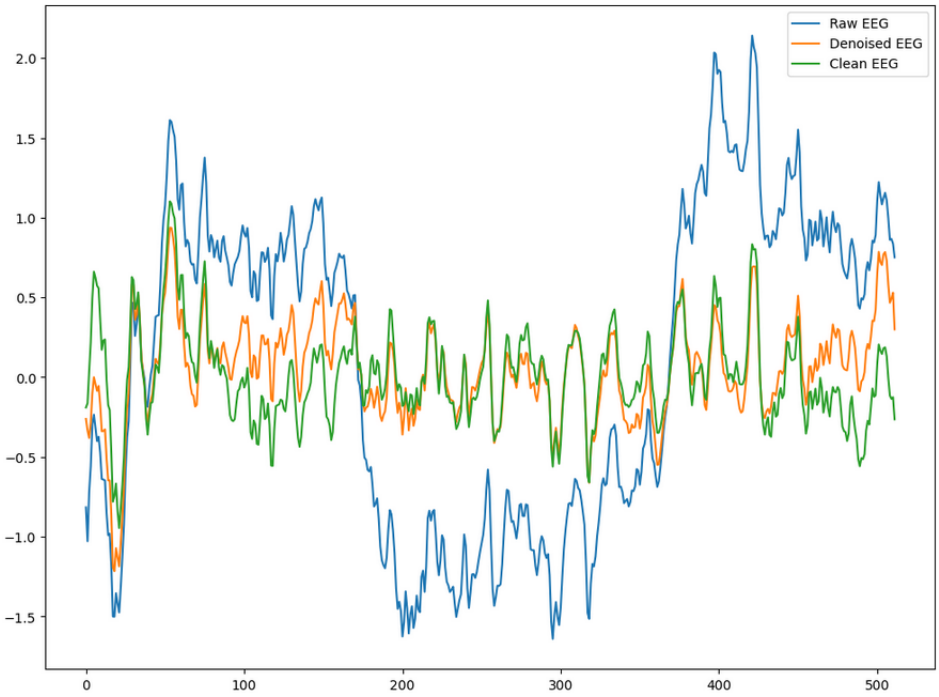

FIGURE 4.8 – Model testing on a contaminated EEG signal with EMG artifacts with, **Blue** is the Raw EEG to be cleaned, **Orange** : The estimated signal, **Green** : Ground truth signal.

4.2.3 Conclusion

This study has demonstrated the effectiveness of a deep convolutional neural network (Deep CNN) model for purifying EEG signals from EOG and EMG artifacts. The model achieved impressive performance, resulting in significantly improved signal quality. This was evidenced by the graphs showing the convergence of the model 4.6, and the model testing on various EEG signals contaminated with different artifacts 4.7, 4.8. Furthermore, the low mean squared error (MSE) rate of approximatley 0.08 underlines the model's strong capability to accurately reconstruct the underlying brain activity

from raw EEG data. These findings suggest that deep learning approaches like Deep CNNs hold great promise for advancing EEG signal processing and enabling more reliable analysis of brain functions in various applications.

4.3 CycleGAN for EEG artifact Removal

Cycle-Consistent Generative Adversarial Networks (CycleGANs). Originally developed for image-to-image translation tasks, CycleGANs can learn to transform data from one domain to another without the need for paired examples. This capability makes CycleGAN a powerful tool for denoising EEG signals by effectively separating the artifact components from the neural signals, thereby improving the signal quality for subsequent analysis.

In this section, we will use the CycleGAN Architecture presented in 3.3, and perform a data preparation for our image dataset, to train the model and finally investigate the overall performance for our Method.

4.3.1 Dataset Preparation

For the studied dataset, we will be using the previous signals dataset EEGDenoise Dataset 4.2.1, select a batch for training and testing. then translating these signals into images to train our models.

Original Signals from the previous dataset are divided into 3 different sets for the signals, EEG, EOG, EMG sets. The following algorithm will explain how the data preparation workflow process will occur :

```
def translate_images(EEG, EOG, EMG):
    # Load the signals
    EEG_with_EMG = EEG + X * EMG # where X is the relative contribution of
                                    the artifact to EEG
    EEG_with_EOG = EEG + X * EOG
    for i in range(1900): #1900 is the number of the training examples we
                                    will generate for our model to
                                    train on
        for i in range(2): # to divide the signal into two chunks of 1x256
                                        samples
        EMG_window = EEG_with_EMG[i][j*256: (j+1)*256]
        EMG_window = EEG_with_EOG[i][j*256: (j+1)*256]

        EMG_Image = Sig_To_image(EMG_window)
        EOG_Image = Sig_To_image(EOG_window)
        # Then we save the images into our local directory
        Save(EMG_Image), Save(EOG_Image)
    # Now for the testing Set we generate 200 images
    for i in range(100): #100 is the number of the testing examples we will
                                    generate for our model to test on
                                    for both spacces (Clean and Noisy)
        for i in range(2): # to divide the signal into two chunks of 1x256
                                        samples
        EMG_window = EEG_with_EMG[i][j*256: (j+1)*256]
        EMG_window = EEG_with_EOG[i][j*256: (j+1)*256]

        EMG_Image = Sig_To_image(EMG_window)
        EOG_Image = Sig_To_image(EOG_window)
        # Then we save the images into our local directory
        Save(EMG_Image), Save(EOG_Image)
```

the function Sig_to_image is :

$$SigToimage[i,j] = floor((Sig[i] + Sig[j]) * 128).$$

The following tables resumes the dataset distribution for training CycleGAN on removing EMG and EOG separatley :

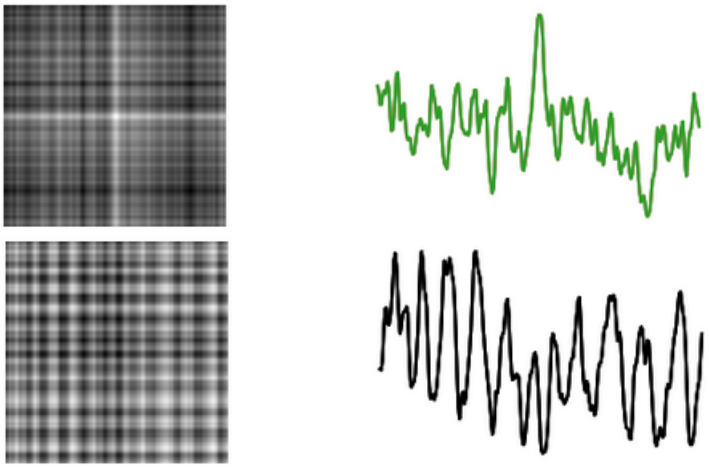

FIGURE 4.9 – Signal translation to image example using the previous algorithm.

TABLE 4.2 – Train/Test distribution for training and testing cyclegan in removing EOG artifacts.

Space	Train	Test
EEG + EOG	1575	125
Clean EEG	1575	125

TABLE 4.3 – Train/Test distribution for training and testing cyclegan in removing EMG artifacts.

Space	Train	Test
EEG + EMG	450	100
Clean EEG	450	100

4.3.2 Experimental results

We trained CycleGAN for 125 epochs on dataset consisting of EEG with EOG artifacts images, the following figures describe the overall loss over the epochs. 4.21 We also tried the trained model

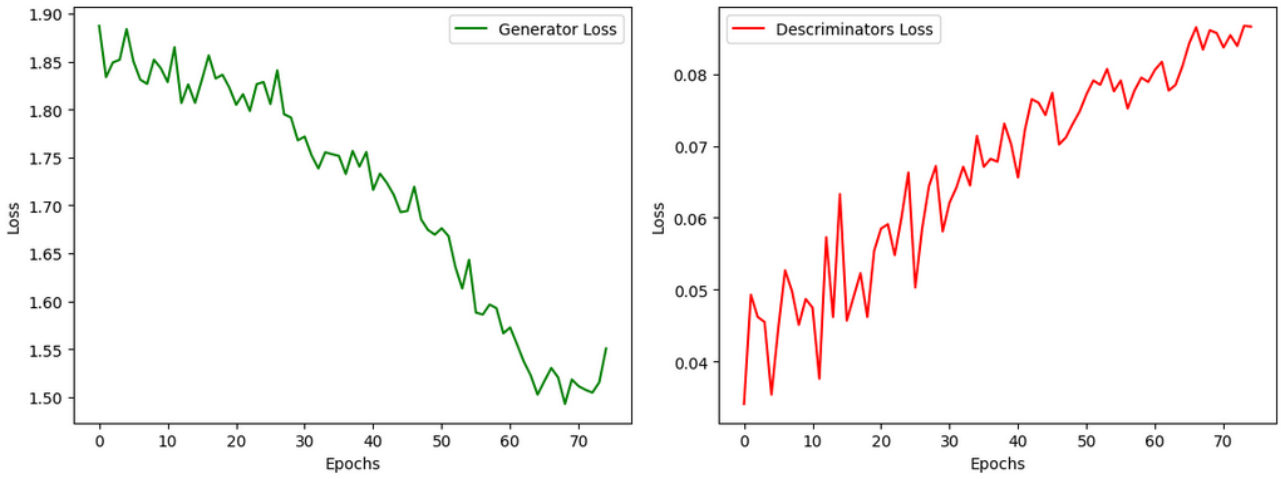

FIGURE 4.10 – Generators, and Descriminators losses.

in testing to see if there is any results, we also introduce numerical results to discuss the model performance for EOG artifacts removal (See figure 4.12) :

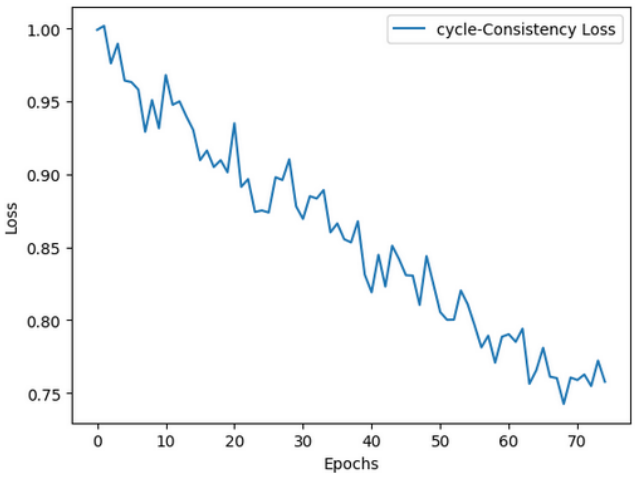

FIGURE 4.11 – Cycle Consistency loss.

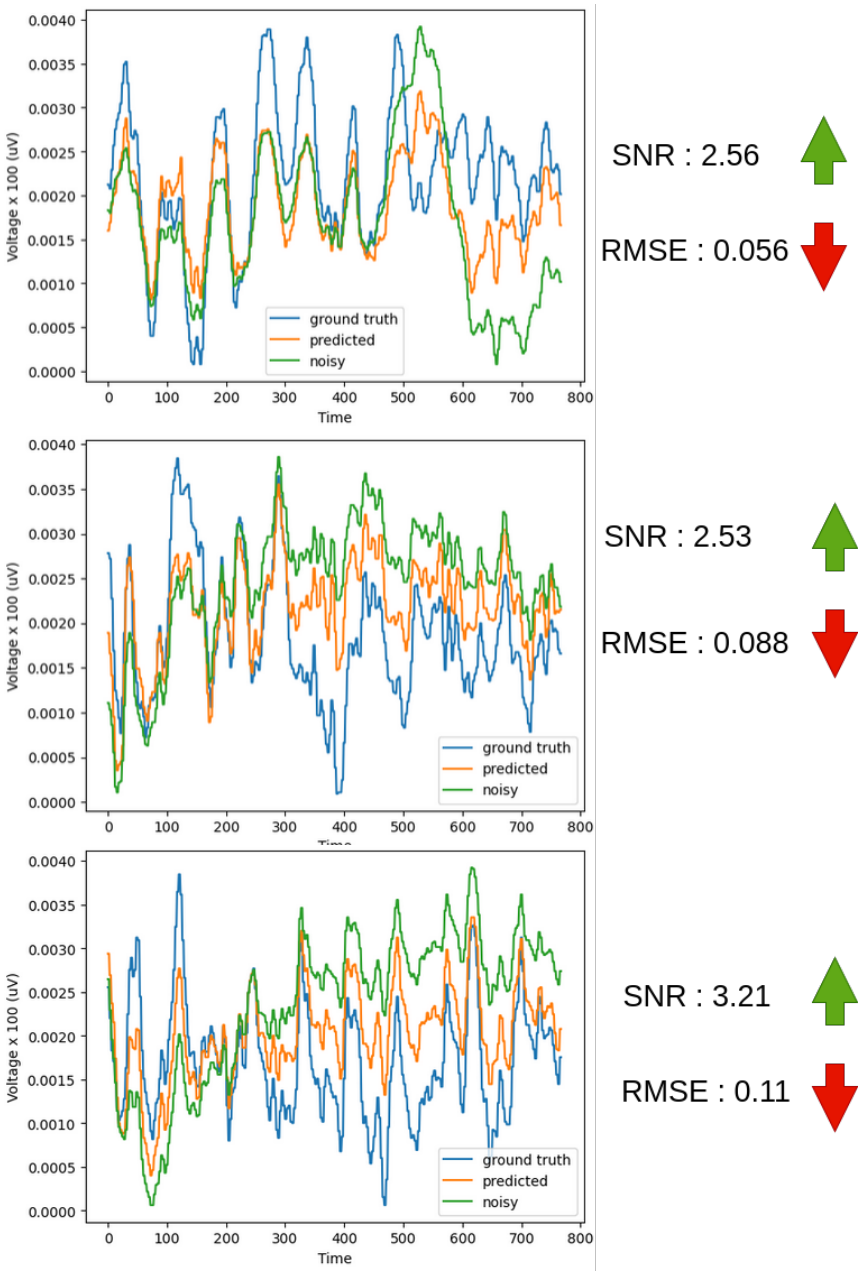

FIGURE 4.12 – Model performance over three samples of the testing test.

However, we trained another model for removing **EMG** artifacts for about 100 epochs and the overall losses were as follows : We also tried the trained model in testing to see if there is any results, we also

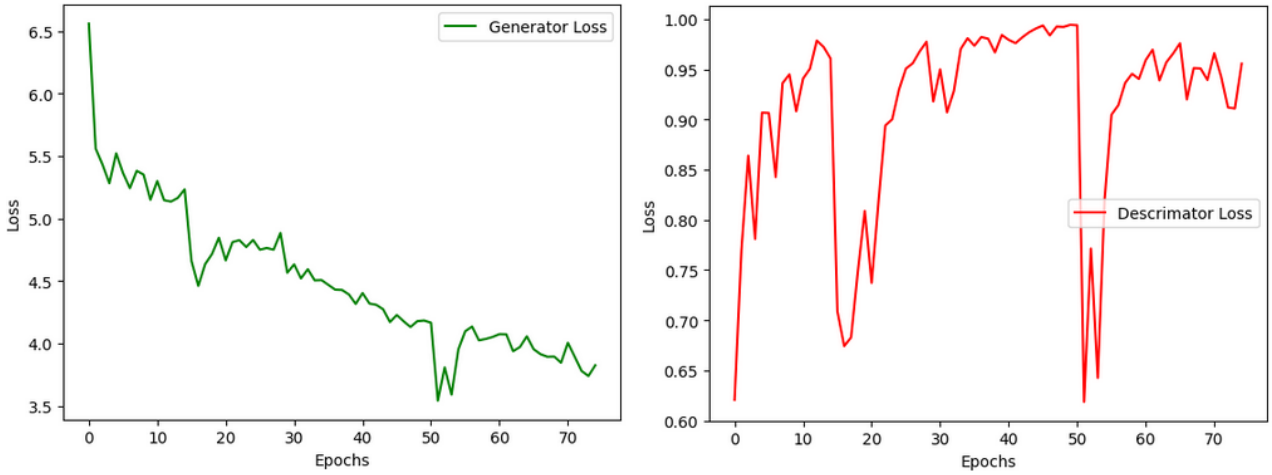

FIGURE 4.13 – Generators, and Descriminators losses.

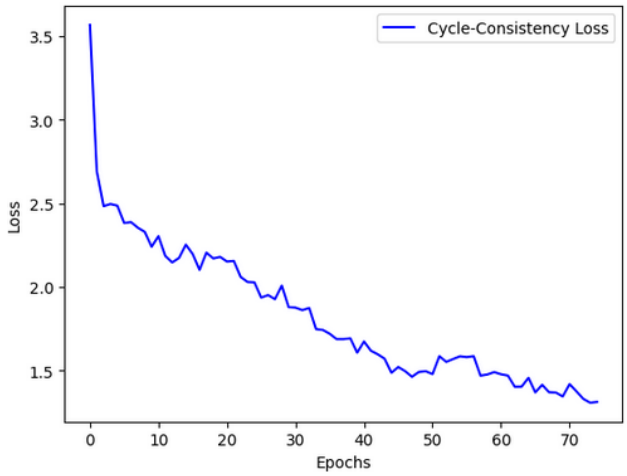

FIGURE 4.14 – Cycle Consistency loss.

introduce numerical results to discuss the model performance for EMG artifacts removal (See figure 4.15) :

4.3.3 Discussion

In this section, we explored the application of CycleGANs to the challenging problem of artifact removal in biomedical signals, specifically targeting electrooculogram (EOG) and electromyogram (EMG) interferences. The experimental results demonstrate that CycleGAN has substantial potential in effectively mitigating these artifacts, leading to cleaner and more interpretable signals.

The preliminary results are indeed promising, indicating that CycleGAN can outperform traditional artifact removal methods in several key aspects, including preserving the underlying physiological signal and minimizing distortion. The neural network's ability to learn intricate patterns and adapt to the complexities inherent in EOG and EMG artifacts showcases its robustness and versatility.

However, the investigation also revealed several areas where further improvements can significantly enhance the efficacy of the method. One primary area of enhancement is the tuning of hyperparameters. The current settings, while functional, suggest that optimal configurations could yield even better

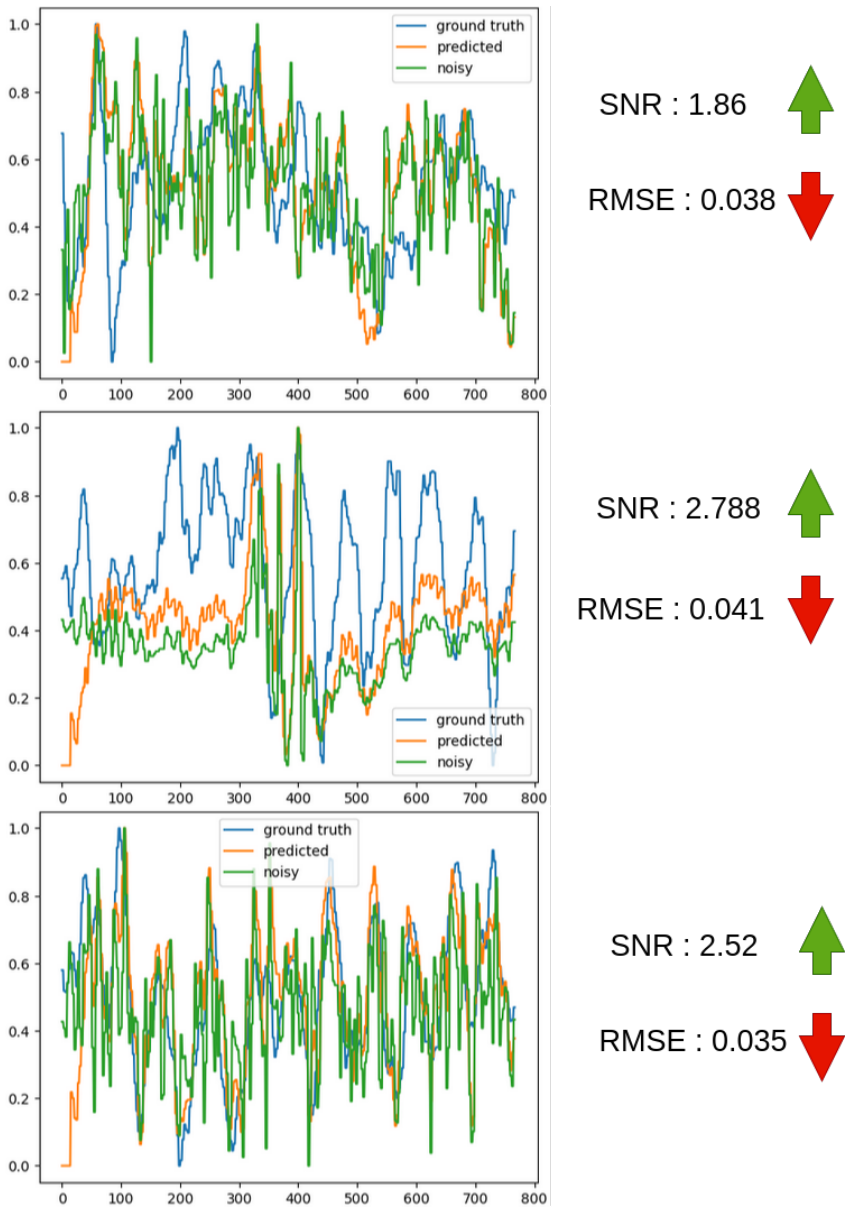

FIGURE 4.15 – Model performance over three samples of the testing test for EMG sets.

performance. Systematic experimentation with hyperparameter values, including learning rates, batch sizes, and network architectures, could provide deeper insights into the ideal operational parameters for artifact removal.

Moreover, the computational power available during this study limited the extent of our exploration. Access to more advanced computational resources would allow for the training of larger and more complex models, potentially capturing more nuanced relationships within the data. This, in turn, would likely lead to even more precise artifact removal and a better understanding of the underlying signal dynamics.

In conclusion, while our findings affirm the capability of CycleGANs in reducing EOG and EMG artifacts, the journey towards optimal implementation is ongoing. Future work should focus on fine-tuning the model parameters and leveraging greater computational power to fully realize the potential of this method. With these advancements, the application of CycleGAN in biomedical signal processing could become a significant tool in enhancing signal quality for various clinical and research purposes.

4.4 CycleGAN for PPG Motion artifacts removal

Motion can corrupt PPG signals, hindering health monitoring. This section investigates using CycleGAN, a deep learning approach, to remove these artifacts. CycleGAN can learn the essence of clean PPG data and remove distortions from motion, potentially offering a sensor-free method for acquiring accurate PPG readings.

Accurately extracting health information from photoplethysmogram (PPG) signals is crucial for wearable health monitoring devices. However, motion artifacts can significantly distort these signals, hindering reliable data acquisition. This section explores the application of CycleGAN, a deep learning technique based on generative adversarial networks (GANs). CycleGAN utilizes two GANs working in tandem to translate PPG signals between two domains : clean and noisy. By learning the underlying characteristics of both clean and motion-corrupted PPG data, CycleGAN can effectively translate noisy signals into their clean counterparts [9], and vice versa. This approach offers a promising avenue for robust PPG signal processing, potentially leading to more accurate health data and improved performance of wearable devices. Thus we will be using the architecture stated in section 3.3

4.4.1 BID-MC Dataset

This study utilizes the BIDMC dataset, a collection of physiological signals and annotations extracted from the MIMIC-II waveform database. The data originates from critically ill patients at Beth Deaconess Medical Center (Boston, MA, USA).

4.4.1.1 Data Collection

The dataset is particularly valuable for researchers developing and evaluating algorithms for respiratory rate estimation. It includes :

- Physiological signals : Electrocardiogram (ECG), pulse oximetry (PPG), and impedance respiratory signals (sampled at 125 Hz).
- Physiological parameters : Heart rate, respiratory rate, and blood oxygen saturation level (sampled at 1 Hz).
- Fixed patient information : Age and gender.
- Manual breath annotations : Provided by two independent annotators for each recording.

The dataset is available in three user-friendly formats : WFDB (standard PhysioNet format), CSV (comma-separated values), and MATLAB (compatible with RRest toolbox).

4.4.1.2 Data Usage

The study case will be mixing motions artifacts with clean PPG segments, the BID-MC dataset has 53 clean PPG signals. Motion artifacts will be acquired from real accelerometer data from existing dataset which is ***Pulse Transit Time PPG Dataset*** [8]. Where three axis (x, y, z) sensor data are available (see figure 4.16)

In our case of study, the three axis data will be summed together using a summing Formula (*7*) then averaged into one signal to represent the motion artifact using the averaging Formula(*8*)

$$Sum = max(|Curr_x - Prev_x|, |Curr_y - Prev_y|, |Curr_z - Prev_z|) \tag{7}$$

$$Avg = 0.9 * Avg + 0.1 * \frac{Sum}{32} \tag{8}$$

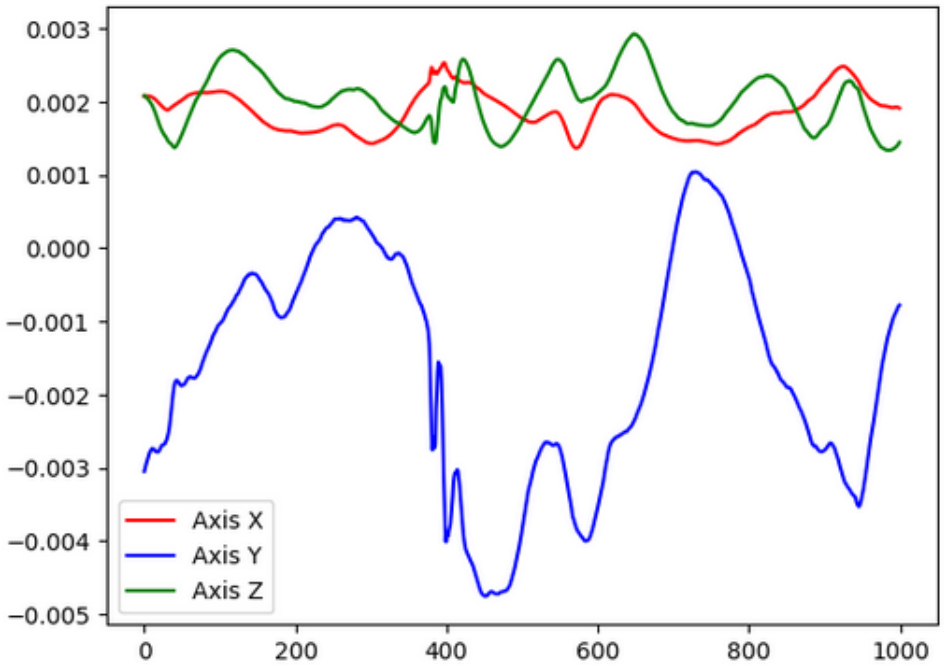

FIGURE 4.16 – PPG Pulse-time transit accelerometer sample signals [8]

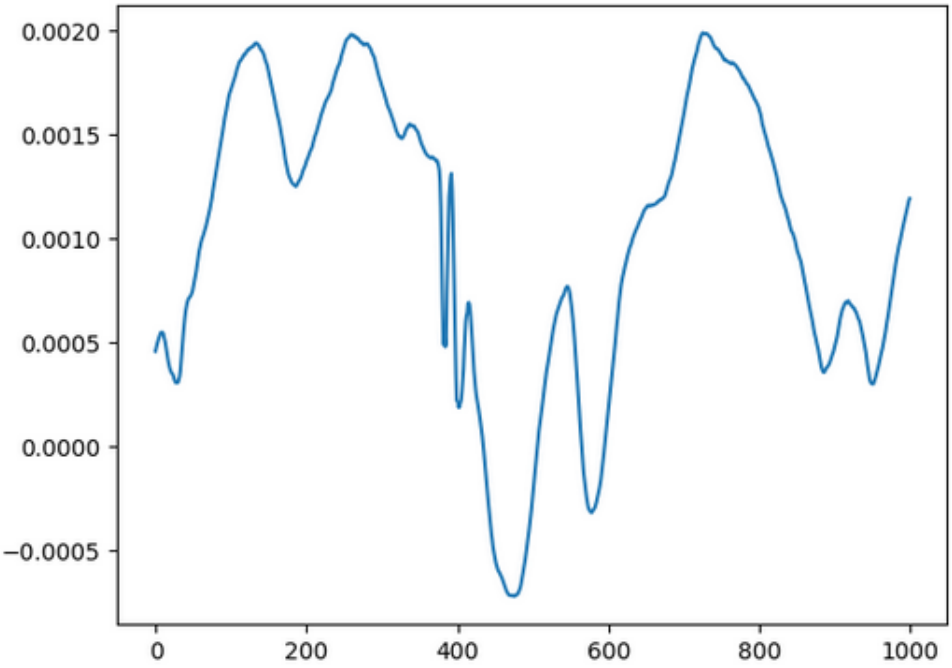

FIGURE 4.17 – Average summing of the 3 axis accelerometer data using 8

Thus, the averaged summing of the three axis accelerometer data should look as follows 4.17 :

Next, clean PPG signals from BID-MC dataset will be segmented into 256 windows and **resampled to the same frequency** as the accelerometer data to ensure the synchronization between the PPG signals and the accelerometer data, then the Averaged accelerometer data will be added to clean PPG data linearly using the following formula :

$$CorruptedSig = X + y.$$

where X is the clean resampled PPG windows, and y is the averaged accelerometer data. and finally the corrupted PPG windowed will be normalized and we shall pass to data preparation section.4.18

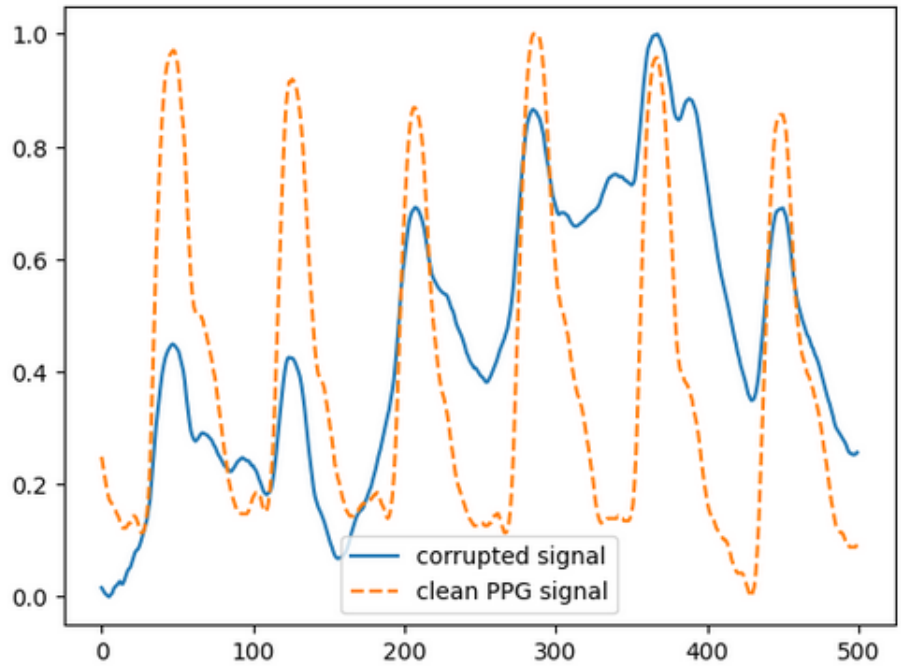

FIGURE 4.18 – The result of adding clean PPG signal with motion artifacts using a linear formula.

4.4.1.3 Data Preparation

The preprocessed signals now will be translated to 2D representation using the translation formula (9)

$$img[i,j] = floor((Sig[i] + Sig[j]) * 128) \tag{9}$$

Where Sig is the normalized window of the signal. thus it will result in a 2D representation for the signals both clean and corrupted ones in a gray scale images. 4.19

Final dataset can be resumed using the following table 4.4

TABLE 4.4 – Train/Test distribution

Space	Train	Test
A (Clean PPG)	900 Images	399 Images
B (Noisy PPG)	900 Images	399 Images

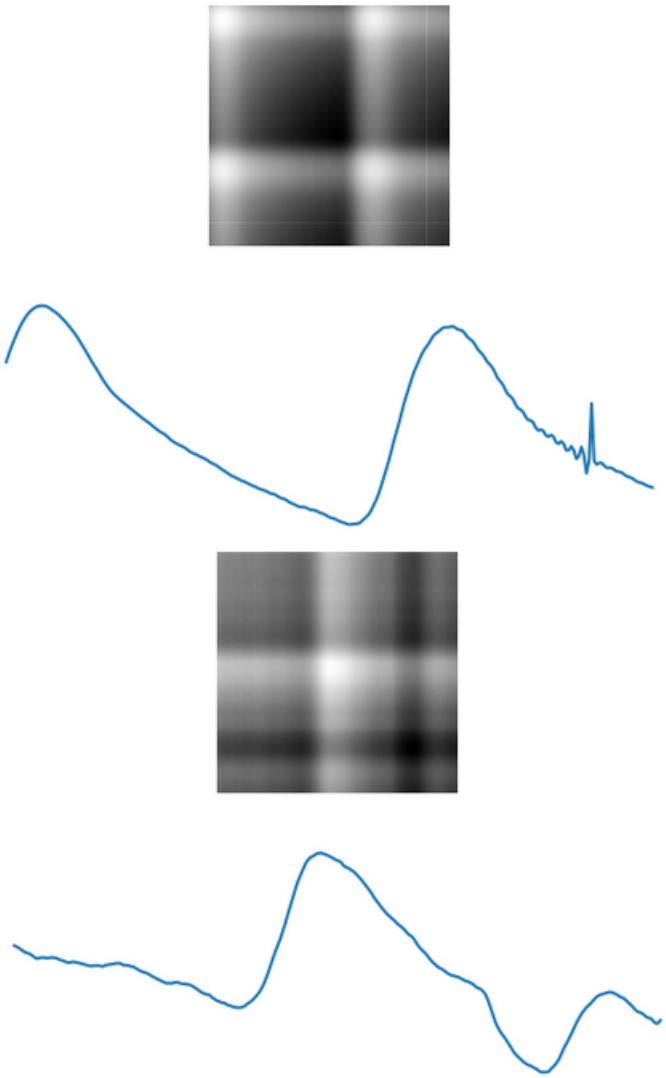

FIGURE 4.19 – Clean and corrupted signal windows with their respctive image representations using the previous formula.

4.4.2 Experimental results

After training the model for 100 epochs, the CycleGAN losses are as follows,

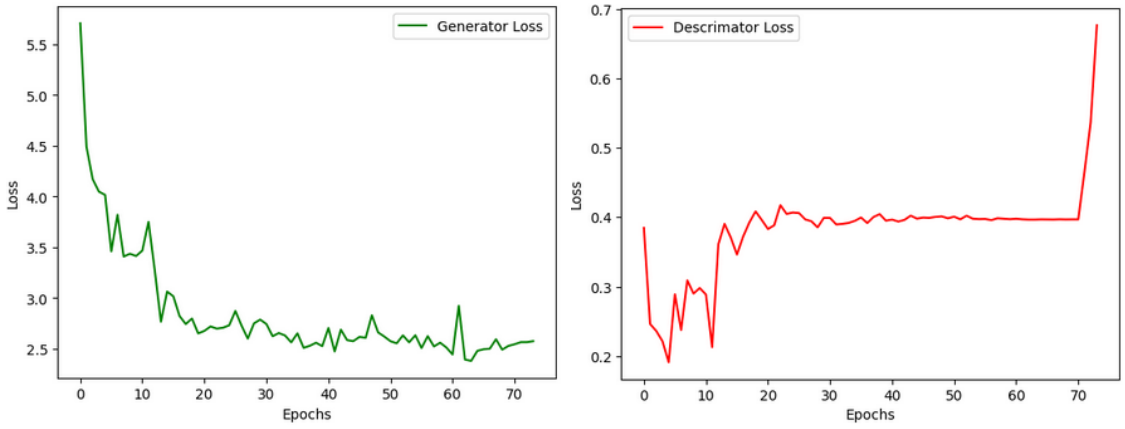

FIGURE 4.20 – Generators, and Descriminators losses.

We also tried the trained model in testing to see if there is any results, we also introduce numerical results to discuss the model performance for motion artifact removal where the improvements are

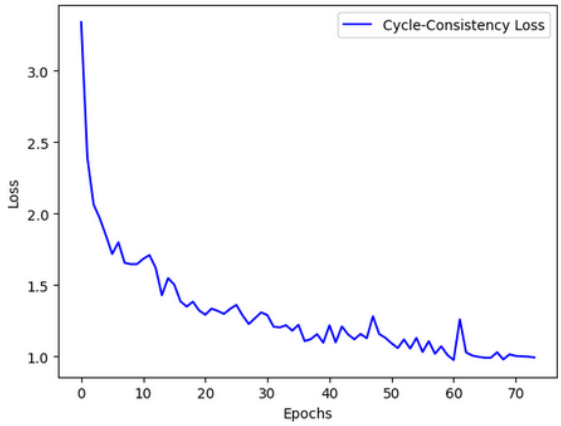

FIGURE 4.21 – Cycle Consistency loss.

measured using **SNR** metric with the unit of Decibel (db) and the **RMSE** to measure the standard deviation between the ground truth signal and the estimated signal, (See figure 4.22) :

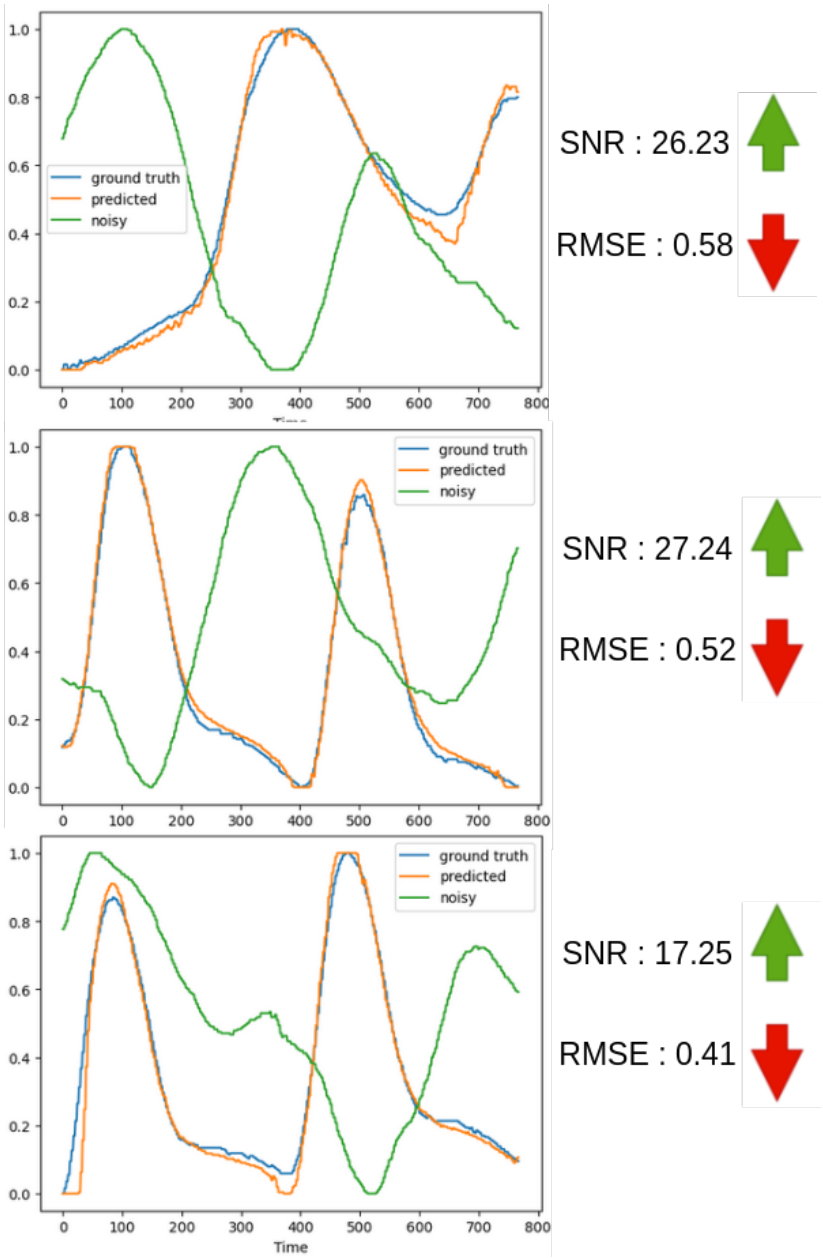

FIGURE 4.22 – Model performance for 3 testing samples for PPG motion artifact removal.

4.4.3 Conclusion

In conclusion, CycleGAN has demonstrated remarkable efficacy for PPG motion artifact removal. By leveraging the power of adversarial training and cycle consistency, CycleGAN effectively learns to map the distorted PPG signals with artifacts to clean signals without the need for paired training data. This ability not only showcases its adaptability but also underscores its potential for real-world applications where acquiring large-scale paired datasets is often impractical or impossible. The consistent reduction in artifacts across diverse datasets and scenarios substantiates CycleGAN's robustness and reliability.

Moving forward, further optimizations and refinements could enhance its performance even more, making CycleGAN a promising tool in biomedical signal processing for improving the accuracy and reliability of physiological measurements.

General Conclusion

One of the main challenges in the field of biomedical signal processing is the elimination of artifacts from PPG and EEG signals. These signals can be severely contaminated by artifacts originating from many sources, making correct analysis and interpretation difficult. While somewhat successful, traditional techniques for removing artifacts from data frequently cannot handle the complexity and variety of real-world data.

To tackle this problem, Deep Convolutional Neural Networks (Deep CNNs) and Cycle-Consistent Generative Adversarial Network (CycleGAN) have become effective tools. By taking advantage of these deep learning approaches' strong feature extraction and data augmentation capabilities, EEG and PPG signals have demonstrated impressive promise in being cleaned up from artifacts.

Deep CNNs, with their hierarchical structure, excel at capturing intricate patterns in data. They have been successfully applied to EEG artifact removal, demonstrating superior performance compared to traditional methods. By learning to distinguish between true neural signals and artifacts, Deep CNNs can significantly enhance the quality of EEG recordings, facilitating more accurate diagnostics and research.

CycleGANs offer a novel approach to artifact removal by learning to translate contaminated signals into clean versions without requiring paired datasets. This makes them particularly useful for biomedical applications where obtaining perfectly clean signals is challenging. CycleGANs have shown great potential in purifying EEG signals, achieving results that outperform many state-of-the-art methods. The ability of CycleGANs to maintain the integrity of the original signal while removing artifacts is a significant advancement, paving the way for more reliable neurophysiological assessments.

Nonetheless, CycleGAN training is a difficult and resource-intensive procedure. Large quantities of memory and high-performance GPUs are among the computing resources needed for it. In addition, precise hyperparameter tweaking and a substantial amount of data are required for the training procedure. Although these demands present difficulties, they are warranted by the improved performance and possible advantages of clearer, more precise messages.

CycleGANs have also shown outstanding performance in the context of PPG signals. CycleGANs have outperformed other cutting-edge approaches as well as conventional methods by efficiently eliminating motion artifacts and other interferences. The accuracy of cardiovascular parameter monitoring may increase as a result of this improvement in signal quality, strengthening the validity of PPG-based health assessments.

The research behind CycleGANs is particularly promising, with ongoing advancements continually improving their efficacy and applicability. Their success in artifact removal for both EEG and PPG signals highlights their potential to revolutionize biomedical signal processing. As these methods continue to evolve, they hold the promise of setting new standards in the accuracy and reliability of neurophysiological signal analysis.

Future Perspectives :

Looking ahead, several exciting avenues exist for the continued development and application of deep

learning techniques in artifact removal for EEG and PPG signals. Future research can explore the following directions :

- Improved Computational Efficiency : Developing more efficient training algorithms and leveraging advancements in hardware can help mitigate the high computational costs associated with training CycleGANs and Deep CNNs. This could make these methods more accessible for widespread use.
- Real-Time Processing : Enhancing these models to operate in real-time can significantly benefit applications such as continuous health monitoring and real-time neurofeedback. Achieving this will require further optimization of model architectures and processing pipelines.
- Multi-Modal Integration : Combining EEG and PPG signals with other physiological data (e.g., ECG, EMG) using multi-modal deep learning approaches can provide a more comprehensive understanding of physiological states and improve artifact removal performance.
- Personalized Models : Developing personalized artifact removal models tailored to individual characteristics can enhance the accuracy and effectiveness of these techniques. This could involve incorporating personalized calibration data during the training phase.
- Clinical Validation : Conducting extensive clinical trials and validations to ensure the robustness and reliability of these methods in diverse real-world settings. This will help in gaining regulatory approvals and fostering adoption in clinical practice.

In conclusion, a major advancement in biomedical signal processing has been made with the use of Deep CNNs and CycleGANs in the artifact removal for EEG and PPG signals. These deep learning methods improve the quality and interpretability of these crucial signals by providing strong answers to the long-standing problem of artifact contamination. These techniques are anticipated to lead to future breakthroughs in the field of biomedical research and diagnostics, despite the significant computer resources needed for training. As such, they are crucial tools.

References

[1] Mars 2014. URL : https://physionet.org/content/ecgiddb/1.0.0/.

[2] Oct. 2023. URL : https://en.wikipedia.org/wiki/Electrooculography.

[3] https://www.researchgate.net/figure/An-illustration-of-EEG-recording_fig2_352194219. [Accessed 17-04-2024].

[4] URL : https://www.sciencedirect.com/book/9780128233740/photoplethysmography.

[5] URL : https://www.telecarechoice.co.uk/oxygen-levels/.

[6] URL : https://www.sciencedirect.com/topics/mathematics/discrete-wavelet-transform.

[7] URL : https://www.researchgate.net/figure/Daubechies-Wavelet-Families-16_fig1_322244768.

[8] URL : https://physionet.org/content/pulse-transit-time-ppg/1.0.0/.

[9] Amir Hosein Afandizadeh Zargari et al. "An Accurate Non-accelerometer-based PPG Motion Artifact Removal Technique using CycleGAN". In : *ACM Trans. Comput. Healthcare* 4.1 (fév. 2023). DOI : 10.1145/3563949. URL : https://doi.org/10.1145/3563949.

[10] Qingsong Ai et al. "Chapter 2 - State-of-the-Art". In : *Advanced Rehabilitative Technology*. Sous la dir. de Qingsong Ai et al. Academic Press, 2018, p. 11-32. ISBN : 978-0-12-814597-5. DOI : https://doi.org/10.1016/B978-0-12-814597-5.00002-3. URL : https://www.sciencedirect.com/science/article/pii/B9780128145975000023.

[11] John Allen. "Photoplethysmography and its application in clinical physiological measurement". In : *Physiological Measurement* 28.3 (fév. 2007), R1. DOI : 10.1088/0967-3334/28/3/R01. URL : https://dx.doi.org/10.1088/0967-3334/28/3/R01.

[12] John Allen. "Photoplethysmography and its application in clinical physiological measurement". In : *Physiological Measurement* 28.3 (fév. 2007), R1. DOI : 10.1088/0967-3334/28/3/R01. URL : https://dx.doi.org/10.1088/0967-3334/28/3/R01.

[13] Matthew Anderson, Tülay Adali et Xi-Lin Li. "Joint Blind Source Separation With Multivariate Gaussian Model : Algorithms and Performance Analysis". In : *IEEE Transactions on Signal Processing* 60.4 (2012), p. 1672-1683. DOI : 10.1109/TSP.2011.2181836.

[14] A. Belouchrani et A Cichocki. "Robust whitening procedure in blind source separation context". In : *Electronics Letters* 36.24 (jan. 2000), p. 2050-2050. DOI : https://doi.org/10.1049/el:20001436.

[15] Hans Berger. "Über das Elektrenkephalogramm des Menschen". In : *Archiv für Psychiatrie und Nervenkrankheiten* 87.1 (déc. 1929), p. 527-570. DOI : https://doi.org/10.1007/bf01797193.

[16] Anita Biswas, Monalisa Singha Roy et Rajarshi Gupta. "Motion Artifact Reduction from Finger Photoplethysmogram Using Discrete Wavelet Transform". In : *Advances in intelligent systems and computing* (mai 2018), p. 89-98. DOI : https://doi.org/10.1007/978-981-10-8863-6_10.

[17] *central limit theorem*$_2$024. Mars 2024. URL : https://en.wikipedia.org/wiki/Central_limit_theorem#.

[18] Xun CHEN et al. "A Preliminary Study of Muscular Artifact Cancellation in Single-Channel EEG". In : *Sensors* 14.10 (oct. 2014), p. 18370-18389. DOI : https://doi.org/10.3390/s141018370.

[19] Xun CHEN et al. "A Preliminary Study of Muscular Artifact Cancellation in Single-Channel EEG". In : *Sensors* 14.10 (oct. 2014), p. 18370-18389. DOI : https://doi.org/10.3390/s141018370.

[20] Juan CHENG et al. *Remove Diverse Artifacts Simultaneously From a Single-Channel EEG Based on SSA and ICA : A Semi-Simulated Study*. 2019. DOI : 10.1109/ACCESS.2019.2915564.

[21] Wikipedia CONTRIBUTORS. *Electromyography*. Sept. 2019. URL : https://en.wikipedia.org/wiki/Electromyography.

[22] Wikipedia CONTRIBUTORS. *Independent component analysis*. Oct. 2019. URL : https://en.wikipedia.org/wiki/Independent_component_analysis.

[23] Arnaud DELORME, Terrence SEJNOWSKI et Scott MAKEIG. "Enhanced detection of artifacts in EEG data using higher-order statistics and independent component analysis". In : *NeuroImage* 34.4 (fév. 2007), p. 1443-1449. DOI : https://doi.org/10.1016/j.neuroimage.2006.11.004.

[24] Maria Camila GUERRERO, Juan Sebastián PARADA et Helbert Eduardo ESPITIA. "EEG signal analysis using classification techniques : Logistic regression, artificial neural networks, support vector machines, and convolutional neural networks". In : *Heliyon* 7.6 (juin 2021), e07258. DOI : https://doi.org/10.1016/j.heliyon.2021.e07258.

[25] Friman O ;Borga M ;Lundberg P ;Knutsson H ; *Exploratory fmri analysis by Autocorrelation Maximization*. URL : https://pubmed.ncbi.nlm.nih.gov/12030831/.

[26] Shao HANYU et Chen XIAOHUI. "Motion artifact detection and reduction in PPG signals based on statistics analysis". In : *2017 29th Chinese Control And Decision Conference (CCDC)*. 2017, p. 3114-3119. DOI : 10.1109/CCDC.2017.7979043.

[27] Hans HERRMANN et Hartmut EWALD. In : *Current Directions in Biomedical Engineering* 7.2 (2021), p. 143-146. DOI : doi:10.1515/cdbme-2021-2037. URL : https://doi.org/10.1515/cdbme-2021-2037.

[28] Harold HOTELLING. *Relations Between Two Sets of Variates on JSTOR — jstor.org*. https://www.jstor.org/stable/2333955. [Accessed 16-04-2024]. 1936.

[29] Norden E. HUANG et al. "The empirical mode decomposition and the Hilbert spectrum for nonlinear and non-stationary time series analysis". In : *Proceedings of the Royal Society of London. Series A : Mathematical, Physical and Engineering Sciences* 454.1971 (mars 1998), p. 903-995. DOI : https://doi.org/10.1098/rspa.1998.0193.

[30] Taesu KIM, Torbjørn ELTOFT et Te-Won LEE. *Independent Vector Analysis : An Extension of ICA to Multivariate Components*. Undetermined. DOI : 10.1007/11679363_21.

[31] Scott MAKEIG et al. *Independent Component Analysis of Electroencephalographic Data*. 1995. URL : https://papers.nips.cc/paper_files/paper/1995/hash/754dda4b1ba34c6fa89716b85d6853Abstract.html.

[32] Najmeh MASHHADI et al. "Deep learning denoising for EOG artifacts removal from EEG signals". In : *2020 IEEE Global Humanitarian Technology Conference (GHTC)*. 2020, p. 1-6. DOI : 10.1109/GHTC46280.2020.9342884.

[33] Mariyadasu Mathe, M. Padmaja et Battula Tirumala Krishna. “Intelligent approach for artifacts removal from EEG signal using heuristic-based convolutional neural network”. In : *Biomedical Signal Processing and Control* 70 (sept. 2021), p. 102935. doi : https://doi.org/10.1016/j.bspc.2021.102935.

[34] Elisa Mejía-Mejía et al. “4 - Photoplethysmography signal processing and synthesis”. In : *Photoplethysmography*. Sous la dir. de John Allen et Panicos Kyriacou. Academic Press, 2022, p. 69-146. isbn : 978-0-12-823374-0. doi : https://doi.org/10.1016/B978-0-12-823374-0.00015-3. url : https://www.sciencedirect.com/science/article/pii/B9780128233740000153.

[35] Bogdan Mijović et al. “Source Separation From Single-Channel Recordings by Combining Empirical-Mode Decomposition and Independent Component Analysis”. In : *IEEE Transactions on Biomedical Engineering* 57.9 (sept. 2010), p. 2188-2196. doi : https://doi.org/10.1109/tbme.2010.2051440.

[36] Gao J ;Zheng C ;Wang P ; *Online removal of muscle artifact from electroencephalogram signals based on canonical correlation analysis*. url : https://pubmed.ncbi.nlm.nih.gov/20307017/.

[37] Junyung Park et al. “Photoplethysmogram Analysis and Applications : An Integrative Review”. In : *Frontiers in Physiology* 12 (mars 2022). doi : https://doi.org/10.3389/fphys.2021.808451.

[38] Kyle Pearce. *Understanding Brain Waves : Beta, Alpha, Theta, Delta + Gamma*. Oct. 2022. url : https://www.diygenius.com/the-5-types-of-brain-waves/.

[39] Marco A. F. Pimentel et al. “Toward a Robust Estimation of Respiratory Rate From Pulse Oximeters”. In : *IEEE Transactions on Biomedical Engineering* 64.8 (août 2017), p. 1914-1923. doi : https://doi.org/10.1109/TBME.2016.2613124. url : https://ieeexplore.ieee.org/abstract/document/7748483.

[40] David Pollreisz et Nima TaheriNejad. “Detection and Removal of Motion Artifacts in PPG Signals”. In : *Mobile Networks and Applications* (août 2019). doi : https://doi.org/10.1007/s11036-019-01323-6.

[41] Thea Radüntz. “Biophysiological Mental-State Monitoring during Human-Computer Interaction”. In : (sept. 2021). doi : https://doi.org/10.18452/23026.

[42] Thea Radüntz. “Signal Quality Evaluation of Emerging EEG Devices”. In : *Frontiers in Physiology* 9 (2018). issn : 1664-042X. doi : 10.3389/fphys.2018.00098. url : https://www.frontiersin.org/journals/physiology/articles/10.3389/fphys.2018.00098.

[43] De Clercq W ;Vergult A ;Vanrumste B ;Van Paesschen W ;Van Huffel S ; *Canonical correlation analysis applied to remove muscle artifacts from the Electroencephalogram*. url : https://pubmed.ncbi.nlm.nih.gov/17153216/.

[44] *Système 10-20 (EEG) — wikimedi.ca*. [Accessed 17-04-2024].

[45] Contributeurs aux projets Wikimedia. *représentation graphique de l’activité électrique du cœur*. Nov. 2003. url : https://fr.wikipedia.org/wiki/%C3%89lectrocardiographie.

[46] Wikipedia contributors. *NumPy — Wikipedia, The Free Encyclopedia*. [Online ; accessed 18-May-2024]. 2024. url : https://en.wikipedia.org/w/index.php?title=NumPy&oldid=1216944842.

[47] Wikipedia contributors. *Pandas (software) — Wikipedia, The Free Encyclopedia*. [Online ; accessed 18-May-2024]. 2024. url : https://en.wikipedia.org/w/index.php?title=Pandas_(software)&oldid=1219216473.

[48] Wikipedia contributors. *PyTorch — Wikipedia, The Free Encyclopedia*. [Online ; accessed 18-May-2024]. 2024. URL : https://en.wikipedia.org/w/index.php?title=PyTorch&oldid=1223171021.

[49] Wikipedia contributors. *Signal-to-noise ratio — Wikipedia, The Free Encyclopedia*. [Online ; accessed 4-June-2024]. 2024. URL : https://en.wikipedia.org/w/index.php?title=Signal-to-noise_ratio&oldid=1219833897.

[50] ZHAOHUA WU et NORDEN E. HUANG. "ENSEMBLE EMPIRICAL MODE DECOMPOSITION : A NOISE-ASSISTED DATA ANALYSIS METHOD". In : *Advances in Adaptive Data Analysis* 01.01 (jan. 2009), p. 1-41. DOI : https://doi.org/10.1142/s1793536909000047.

[51] Haoming Zhang et al. *EEGdenoiseNet : A benchmark dataset for end-to-end deep learning solutions of EEG denoising*. 2021. arXiv : 2009.11662 [eess.SP].

[52] Jeremy Zhang. *UNet Line by Line Explanation*. Oct. 2019. URL : https://towardsdatascience.com/unet-line-by-line-explanation-9b191c76baf5.

[53] Jun-Yan Zhu et al. *Unpaired Image-to-Image Translation using Cycle-Consistent Adversarial Networks*. 2020. arXiv : 1703.10593 [cs.CV].

Appendix

Appendix A

Materials, Tools, and Libraries

1.1 Libraries

1.1.1 Python

Python is an interpreted, multi-paradigm, and cross-platform programming language. It promotes structured imperative, functional, and object-oriented programming. It features strong dynamic typing, automatic memory management via garbage collection, and an exception handling system.

Python was created in 1989 by Guido van Rossum, in the Netherlands. *The name Python comes from a tribute to the television series Monty Python's Flying Circus, of which G. van Rossum is a fan.* The first public version of this language was released in 1991.

1.1.2 Scikit-learn

Scikit-learn is a free Python library designed for machine learning. It is developed by numerous contributors, especially in the academic world.

Within its framework, it offers many pre-implemented algorithm libraries ready to use. These libraries are available particularly to data scientists.

It notably includes functions for estimating random forests, logistic regressions, classification algorithms, and support vector machines (SVM). It is designed to integrate well with other free Python libraries, notably NumPy and Pandas.

1.1.3 PyTorch

PyTorch is a machine learning library based on the Torch library, used for applications such as computer vision and natural language processing, originally developed by Meta AI and now part of the Linux Foundation umbrella. It is recognized as one of the two most popular machine learning libraries alongside TensorFlow, offering free and open-source software released under the modified BSD license.

Although the Python interface is more polished and the primary focus of development, PyTorch also has a C++ interface. [48]

A number of pieces of deep learning software are built on top of PyTorch, including Tesla Autopilot,[13] Uber's Pyro Hugging Face's Transformers, PyTorch Lightning, and Catalyst.

- Tensor computing (like NumPy) with strong acceleration via graphics processing units (GPU)
- Deep neural networks built on a tape-based automatic differentiation system

1.1.4 The incredible pandas

Pandas (styled as pandas) is a software library written for the Python programming language for data manipulation and analysis. In particular, it offers data structures and operations for manipulating numerical tables and time series. It is free software released under the three-clause BSD license. The name is derived from the term "panel data", an econometrics term for data sets that include observations over multiple time periods for the same individuals, as well as a play on the phrase "Python data analysis". *Wes McKinney started building what would become Pandas at AQR Capital while he was a researcher there from 2007 to 2010.*

The development of Pandas introduced into Python many comparable features of working with DataFrames that were established in the R programming language. The library is built upon another library, NumPy. [47]

1.1.5 NumPy

NumPy is a library for the Python programming language, adding support for large, multi-dimensional arrays and matrices, along with a large collection of high-level mathematical functions to operate on these arrays. The predecessor of NumPy, Numeric, was originally created by Jim Hugunin with contributions from several other developers. In 2005, Travis Oliphant created NumPy by incorporating features of the competing Numarray into Numeric, with extensive modifications. NumPy is open-source software and has many contributors. [46]

1.2 Materials (Hardware)

Given the relatively complex nature of our problem, we employed deep neural networks (DNN) for signal reconstruction, some of which had millions of parameters to calibrate during model training. This task thus demands hardware configuration that meets several criteria :

- Sufficient computational power (via CPUs or GPUs).
- Hardware robustness (to prevent interruptions during tasks).
- Adequate storage capacity.

In our project, as with any project involving DNNs, the most resource-intensive task is training the various models. To address this, we utilized several solutions, which are described below :

1.3 Tools (Google Colaboratory)

Colaboratory, often abbreviated as "Colab," is a product of Google Research. Colab allows anyone to write and execute Python code of their choice through the browser. It's a particularly suitable environment for machine learning, data analysis, and education. In more technical terms, Colab is a hosted service for Jupyter notebooks that requires no setup and provides free access to computing resources, including GPUs.

We primarily used Google Colab for relatively simple and short training sessions for several reasons :

- The resources provided by Google are not defined and are fluctuating (thus unstable).
- The quality of the GPUs offered is often relatively low.
- The tool is designed for training sessions lasting no longer than 30 minutes ; the kernel stops after 30 minutes of user inactivity.

For these reasons, we opted for other platforms for larger training sessions.

1.3.0.1 Personal setup

We trained our models on our personal computer which is mainly suitable for Neural networks training and already settled with **Cuda** technology, the following are the computer features :

- **Processor :** Intel I7 10th generation.
- **Graphical card :** RTX 2060 and Tesla V100.
- **RAM :** 42 GB.
- **OS :** Ubuntu 22.02.
- **Storage :** 1TB SSD.